R. & M. No. 3642

MINISTRY OF TECHNOLOGY

AERONAUTICAL RESEARCH COUNCIL
REPORTS AND MEMORANDA

A Low-Speed Wind-Tunnel Investigation of the Tailplane Effectiveness of a Model Representing the Airbus Type of Aircraft

By D. A. LOVELL

Aerodynamics Dept., R.A.E., Farnborough

LONDON: HER MAJESTY'S STATIONERY OFFICE
1970

PRICE £1 2*s.* 0*d.* [£1·10] NET

A Low-Speed Wind-Tunnel Investigation of the Tailplane Effectiveness of a Model Representing the Airbus Type of Aircraft

By D. A. LOVELL

Aerodynamics Dept., R.A.E., Farnborough

Reports and Memoranda No. 3642*
April, 1969

Summary.

Measurements of lift, drag and pitching moment have been made on a model having three tailplane heights and three wing configurations, with and without the tailplane in position. Wake and boundary-layer surveys at the tailplane heights and a separate force and moment test of the isolated tailplane were also made. The results have been analysed to find the tailplane efficiency, as measured by the effective lift-curve slope, for the three tailplane heights tested. The contribution of the mean dynamic pressure at the tailplane to the effective lift-curve slope was removed. The remaining difference in lift-curve slope from that obtained in the separate tailplane test was due to the interference involved in mounting the tailplane on the model. It was found that this interference was negligible for the tailplane mounted away from the body. With the tailplane mounted on the large body, typical of current airbus bodies, the interference was small and no evidence of extensive flow separation was found.

LIST OF CONTENTS

Section

1. Introduction
2. Description of the Model
3. Details of Tests and Reduction of Results
   - 3.1. Complete model force and moment tests
   - 3.2. Wake-traverse and boundary-layer measurements
   - 3.3. Flow visualisation
   - 3.4. Isolated tailplane force and moment test
4. Force and Moment Results
   - 4.1. Clean wing
   - 4.2. Clean wing with high-lift devices
   - 4.3. Extended wing

*Replaces R.A.E. Technical Report No. 69 077—A.R.C. 31 507.

4.4. Isolated tailplane test

5. Wake and Boundary-Layer Traverse and Flow Visualisation Results

5.1. Wake-traverse results

5.2. Boundary-layer traverse results

5.3. Flow visualisation results

6. Tailplane Effectiveness

6.1. The factors determining tailplane effectiveness

6.2. Tailplane efficiency of the present tests

6.3. Other measurements of tailplane efficiency

7. Conclusions

List of Symbols

References

Appendix A

Table 1

Illustrations—Figs. 1 to 33

Detachable Abstract Cards

---

1. *Introduction.*

The function of the tailplane of an aircraft is to provide a sufficient range of pitching moment, throughout the aircraft flight envelope, to trim and control the aircraft in the longitudinal plane. In seeking a solution to this requirement three main factors need to be considered.

(1) The geometrical relation between the tailplane and the wing-body combination (e.g. the ratio of tailplane area to wing area and the tailplane moment arm).

(2) The performance of the tailplane mounted in a given position as compared to its performance in free air (e.g. the lift produced by the tailplane in these two situations).

(3) The structural problems involved in mounting the tailplane in a given position (e.g. providing sufficient stiffness in a fin to support a tailplane on top of the fin without flutter occurring).

The first factor is not considered explicitly in this Report but the variation of the tailplane environment with tailplane height has been investigated. The principal purpose of the present work is to consider (2), the aerodynamic performance of the tailplane, and to establish the efficiency of operation of the tailplane. The breakdown into the effects determining the tailplane effectiveness made by Kirk[1] is still highly relevant and a similar analysis has been made more recently by Neely and Griner[2]. The important factors are:

(a) The effect of the wake of the wing-body combination on the velocity field at the tailplane.

(b) The effect of the fuselage boundary layer.

(c) The interference effect of the fuselage on the tailplane lift distribution.

(d) The downwash field produced at the tailplane by the wing-body combination.

Previous investigations of these factors, many of which are summarised in Ref. 2, have been concerned with either the low aspect-ratio wing, fighter type of aircraft or the high aspect-ratio wing, transport aircraft having relatively small diameter bodies. Analysis of the limited results with a tailplane in an experimental investigation of the aerodynamics of the airbus type of aircraft[3] indicated that the performance of the tailplane might be adversely affected because of the possibility of a large body producing a large interference and flow separation at the tailplane. Accordingly a series of detailed tests were made at three tailplane heights using a model typical of current airbus designs.

Within the limitations of the present work it may be said that there are no new problems posed by large-body aircraft in the realm of tailplane effectiveness. However to calculate tailplane performance requires knowledge of the downwash field at the tailplane which present theoretical methods cannot supply to any great accuracy (e.g. downwash prediction to $\pm 1°$). Furthermore the tailplane effectiveness has only been considered over the normal operating incidence range. The work of Kettle and Kirby[4] indicates that the performance of a tailplane on an aircraft at very high incidence should be examined as the position of the wing, body and nacelle wakes can be a critical factor in determining longitudinal stability at these incidences. In this connection some measurements[5] have been made at very high incidences on an airbus-type of aircraft model.

2. *Description of the Model.*

Fig. 1 shows the general arrangement of the model tested and Table 1 lists the geometric details of the model. The fuselage and tailplane were typical of those in recent proposals for the airbus type of aircraft. Three tailplane heights were used; a fuselage mounting, a mounting on top of the fin, and a mounting midway between these two positions. The horizontal tail arm was kept constant for the three heights of the tailplane. Two tailplanes were made so that the overall span was unchanged for the fuselage and fin mounting positions. A large flat-plate fin was made to accommodate the three mounting positions and prevent any cross flow between the tailplane halves. The leading edge of the 0·25 inch (6·35mm) thick plate was radiused and the trailing edge was left square cut. Provision was made for a range of tailplane geometric settings, i_t, on the fin and body. The method of allowing a range of tail setting on the body was carefully designed so that tailplane movement was possible without the need for a large cutout in the rear fuselage to accommodate the method of adjustment and fixing which might give rise to unwanted surface irregularities.

The wing used on the model was that designed by Kettle[3] for a generalised airbus type of aircraft model. High-lift devices in the form of leading-edge droop and Fowler flaps were fitted to the wing. On the airbus type of aircraft it is common to extend the chord of the wing in the root region mainly in order to accommodate the undercarriage. As it is possible that the change to a kinked planform may produce a very different environment at the tailplane, it was felt desirable to test an alternative planform. Therefore an extension of the wing was made, consisting of a flat plate secured in the flap cavity, which extended the chord so that the wing centreline chord was increased by 33·5 per cent and produced a kink in the planform at 35·7 per cent span. The aerofoil section was formed using plasticine and the section defined as a straight line in the streamwise direction from the point of maximum thickness to the trailing edge. As the main object of the tests was concerned with the tailplane performance it was not felt that the change of section or the relatively poor surface finish obtainable was important.

3. *Details of Tests and Reduction of Results.*

3.1. *Complete Model Force and Moment Tests.*

All the complete model tests were made in the No. 1 $11\frac{1}{2}$ft $\times$ $8\frac{1}{2}$ft low-speed wind tunnel at R.A.E. Farnborough at a wind speed of 140 ft/sec. (42·7 m/s). The standard wire support rig was used with the pitching-moment balance and weight wires attached to the nose rather than the tail of the fuselage in order to minimise the possibility of interference affecting the tailplane performance.

A transition wire was placed round the nose of the fuselage at the position of half maximum diameter. An evaporation technique using a solution of acenaphthalene in petroleum ether was used to check that

transition occurred at the wire at 140 ft/sec. (42·7 m/s). A 24 swg (0·559 mm) wire was found to be satisfactory. The wing, which had been used extensively for the tests of Ref. 3, has suffered some deterioration and was sufficiently rough for transition to be fixed in the vicinity of the leading edge without recourse to any devices. Transition was left free on the tailplane.

Measurements of the three longitudinal components, lift, drag and pitching moment, were made for six model conditions: the clean wing with three tailplane heights, the clean wing with high-lift devices and the low tailplane position and extended wing with high and low tailplane positions. A range of tail setting was covered for each of these conditions. The three components were also measured for the three corresponding conditions without a tailplane. All these measurements were made over a wing incidence range of $-3°$ to $15°$.

The balance output was displayed on a digital voltmeter and the voltage level was automatically coded and output onto paper tape when a balance point had been obtained. A computer programme was used to reduce this output data to corrected coefficients by firstly converting the balance data to force and moment coefficients, secondly correcting the coefficients for the wire support rig contributions and finally correcting the coefficients for the wind-tunnel wall-interference effects.

As it was intended to take differences between the forces and moments measured with and without the tailplane in position, the corrections due to the difference in wind-tunnel wall interference (blockage and lift constraint effects) between the wing and tailplane were carefully examined using the methods discussed in Ref. 6. For the present model the difference in blockage was negligible and the existing method for correcting for the difference in lift constraint could be reduced to the simple relationship:

$$\delta C_m = -\left(\frac{\partial C_m}{\partial i_t}\right)_{\alpha_w} (\Delta\alpha_t - \Delta\alpha_w). \tag{1}$$

For ease of application of this correction it is common to take an average value of the partial derivative $(\partial C_m/\partial i_t)_{\alpha_w}$ over the range of incidence tested but for the present work the value appropriate to the particular incidence is used in order to obtain higher accuracy. Corrections to lift and drag, corresponding to equation (1) for pitching moment, but which are much smaller, have also been applied.

An investigation of the empty tunnel airflow in the vertical plane at the longitudinal position of the tailplane pivot using a pitot-static probe showed variations of up to 1·5 per cent in the dynamic pressure in the region traversed by the tailplane when covering a wing incidence range from $-3°$ to $15°$ for the three tailplane positions. Furthermore there was a variation of up to 1·2 per cent in the dynamic pressure in this region relative to the reference value at the balance centre (at the mid point of the pitching-moment axis and on the tunnel centreline). For each wing incidence a mean dynamic pressure at the tailplane was calculated weighted for the local tailplane chord (which is equivalent to tailplane loading proportional to local chord or constant sectional lift coefficient). The measurements made with a tailplane on the model were corrected for this difference in dynamic pressure from the reference value so that the final coefficients are for the model in a uniform flow.

The pitching-moment coefficients have been referred to a centre at the intersection of the wing mean quarter-chord line and the vertical plane of symmetry of the model.

The greatest source of inaccuracy in the measurements arises from the limited accuracy with which it is possible to measure the wing incidence and tail setting. Repeated measurements of the same angle by different operators, using a telescope which was set up anew for each measurement, showed that a repeatability to within 0·05° could be obtained. Accurate measurement of the tail setting was ensured by scribing an incidence datum on each half of the tailplane and measuring the setting of each tailplane half. The settings quoted in the results are the mean of these two readings. If a typical value of the derivative $(\partial C_m/\partial i_t)_{\alpha_w}$ is taken as $-0·06$ per degree, the 0·05° accuracy of angular measurement will correspond to a variation of pitching moment coefficient of 0·0030.

3.2. *Wake-Traverse and Boundary-Layer Measurements.*

In order to determine the environment in which the tailplane was operating the dynamic pressure was

measured by means of two rakes, one to cover the region removed from the body and the other to measure the boundary layer on the body.

The first rake, of 1·25 ft (0·381 m) span and consisting of eight pitot tubes at intervals of 0·167 ft (0·051 m) interspersed with five static tubes at intervals of 0·333 ft (0·101 m), all the pressure holes being in line, was mounted on the model in place of the tailplane. The rake was so arranged that it pivoted on the tailplane pivot and that all the pressure holes were in line with the tailplane pivot line. Measurements were made for four model conditions; the clean wing, with the rake in the low tailplane position, the clean wing with high-lift devices and the rake in the high and low tailplane positions and the extended wing with the rake in the low tailplane position.

The principle concern of this study of the wing-body wake was the dynamic pressure environment at the tailplane positions tested. Flow direction was therefore not measured and the effect of sidewash on the readings of the simple pivot tubes used was assumed negligible. A simple procedure was adopted to remove the effect of airflow pitch on the reading of the pitot tubes. For each wing incidence of the range tested for each model condition at least three rake settings relative to the body were used in order to determine the true dynamic pressure. The pressure coefficients read from the manometer, which had been set to read coefficients relative to the empty tunnel calibration for total head and static pressure, were corrected for tunnel blockage effect, tunnel flow non-uniformity (from the results mentioned in 3.1) and the rake instrument error (determined by comparing the pressures recorded by the rake and a standard probe in the empty tunnel).

The second rake, a boundary-layer rake of 2 inches (50·8 mm) span consisting of twelve pitot tubes at intervals varying from 0·1 inch (2·5 mm) to 0·25 inch (6·4 mm) and a single static tube in the centre, all the pressure holes being in line, was mounted in place of the tailplane. The rake was screwed to the body so that a line of pressure holes was perpendicular to the surface and this line intersected the surface at the tailplane pivot hole. Measurements were only made with the rake on the body as the boundary layer on the fin was of negligible thickness. Tests were made for the clean wing planform with and without high-lift devices. The boundary-layer rake was set at an angle relative to the body estimated using the results of the wake traverse and the mean downwash derived from the force and moment measurements. One attempt was made at removing the effect of pitch on the pressure readings, by using several settings at one wing incidence, which showed that there was a large variation in downwash near the body and that the single static-pressure tube was insufficient. The results were reduced to velocity profiles using a value for the static-pressure coefficient extrapolated from the wake-traverse results. The accuracy of these boundary-layer results is probably within 1 per cent after allowing for the effects or airflow yaw and pitch relative to the pressure tubes. The results were only corrected for tunnel blockage.

3.3. *Flow Visualisation.*

The airflow over the body with the clean wing and low tailplane was examined by an evaporation technique of flow visualisation using a suspension of fluorescent Dayglo powder in paraffin. The speed was rapidly brought up to 140 ft/sec (42·7 m/s) so that there was no risk of obtaining flow patterns corresponding to lower speeds. After a quarter of an hour at 140 ft/sec (42·7 m/s) the paraffin had completely evaporated. Good photographic results were obtained by blacking out the tunnel and illuminating the model with ultra-violet light so that the only visible light was that produced by the fluorescence.

The flow over the tailplane in the high position, with the clean wing condition, was visualised by another evaporation technique[7] using a suspension of titanium dioxide in paraffin.

3.4. *Isolated Tailplane Force and Moment Tests.*

The tailplane alone was tested in the 4ft × 3ft low-speed wind tunnel at R.A.E. Farnborough at wind-speeds of 80 ft/sec (24·4 m/s), 140 ft/sec (42·7 m/s) and 200 ft/sec (61 m/s). A sting was made of the same thickness as the fin so that the overall span remained unchanged. The sting was located in the two tailplane halves by a dowel and locked in position by the pivot rod used for mounting the tailplane on the fin. Cleats were recessed into the surface at the mean quarter-chord position of the tailplane 0·917 ft (0·280 m) apart. The recesses were made the same above and below the tailplane so that it could be tested

both ways up. The standard arrangement was used for the wire support rig for the model in the tunnel. Measurements of the three longitudinal components, lift, drag and pitching moment, were made over an incidence range of $-3°$ to 18° with the model both ways up. A simple computer programme was used to calculate the coefficients corrected for the effects of the support rig and the wind-tunnel walls. The moments measured were transferred to an axis on the chord line.

4. *Force and Moment Results.*

4.1. *Clean Wing.*

The results for the three tailplane positions are shown in Fig. 2 to Fig. 10 together with the results obtained without a tailplane. The variation of lift coefficient with incidence is shown in Figs. 2, 3 and 4. A partial stall occurs at a wing incidence of 13° which may be a consequence of the poor state of the wing leading edge. It is also apparent that some reduction in the tailplane contribution to the overall lift occurs as the tailplane is moved down the fin, for a constant tail setting.

The variation of drag coefficient with incidence is shown in Figs. 5, 6 and 7. There is a reduction in drag as the tailplane is moved down the fin, for a given tail setting, and the incidence at which minimum drag occurs decreases as the tail setting is increased. The variation of pitching-moment coefficient with lift coefficient is shown in Figs. 8, 9 and 10. The C_m *versus* C_L curves at constant tail setting are not linear even for the high tailplane position and, as the linearity of the C_m *versus* C_L curves at constant wing incidence confirms the experimental accuracy suggested in Section 3.1, this may be due partially to the non-linear variation of the tailplane lift with incidence. This is discussed further in Section 4.4. The slope of the C_m *versus* C_L curves at constant wing incidence is close to the approximate theoretical value (neglecting the tailplane drag contribution to the forces and moments) of $-\frac{l'}{\bar{c}}$ where l' is the tail arm measured in tailplane wind axes and $\bar{c}$ is the mean chord.

With regard to the effectiveness of the tailplane in producing pitching moment to trim or control the aircraft, two trends are apparent as the tailplane is moved down the fin and onto the body. Firstly the mean slope of the C_m *versus* C_L curves at constant tail setting decreases and secondly the curves for a range of tail setting become closer together. These trends which are due principally to the change in the variation of downwash at the tailplane with wing incidence and the change in the dynamic pressure at the tailplane with wing incidence respectively, are discussed further in Section 6.

4.2. *Clean Wing with High-Lift Devices.*

The results, for the wing with leading edge droop of 25° and a Fowler flap deflection of 35°, for the low tailplane position, are shown in Figs. 11 to 13 together with the results obtained without a tailplane. The variation of the drag coefficient with incidence is shown in Fig. 12. Large negative tail settings produce a large increase in drag at low values of wing incidence which is later shown to be due to the tailplane stalling because of the large downwash produced by the high-lift devices. The variation of the pitching-moment coefficient with the lift coefficient is shown in Fig. 13. The large nose-down pitching moment produced by the Fowler flaps can be seen by comparing the no tailplane results with those in Fig. 10. The trends noted in Section 4.1 as the tailplane is moved down the fin and onto the body are continued in this case as can be seen by again comparing the Figs. 10 and 13.

4.3. *Extended Wing.*

The results, for the extended wing and the high and low tailplane positions, are shown in Figs. 14 to 19. The forces and moments are non-dimensionalised with respect to the *area of the clean wing*. The variation of the lift coefficient with incidence is shown in Figs. 14 and 15. Comparing the no-tailplane curves of the extended and clean wings there is a lift increase of 5 per cent produced by a 5 per cent increase in net area outside the body which corresponds to an increase of 11 per cent in the gross area. The variation of the drag coefficient with incidence is shown in Figs. 16 and 17. The minimum drag coefficient is only increased by 0·0008 over the clean-wing result confirming that the crude method of extending the planform had no deleterious effect. Otherwise the results are very similar to those for the plain wing.

4.4. *Isolated Tailplane Test.*

The test results for the tailplane at windspeeds of 80 ft/sec (24·4 m/s), 140 ft/sec (42·7 m/s), and 200 ft/sec (61 m/s) are shown in Figs. 20 to 22. The variation of lift coefficient with incidence, Fig. 20, is non-linear below the stall, the degree of non-linearity decreasing as the speed is increased. This non-linearity of the C_L *versus* α curve has been found before on moderately swept wings; for example Ref. 8, Fig. 3a, shows the variation of lift-curve shape as Reynolds number is increased. Simple sweep theory has been used in the past[8] to estimate the value of C_L at which a kink occurs in the lift curve. Using the two-dimensional data of Ref. 9 a similar estimate was made for the tailplane. Reasonable agreement was obtained for the value of C_L at which the upper kink occurred on the C_L *versus* α curve. The flow visualisation at 140 ft/sec (42·7 m/s) confirmed that the flow was attached at 6° incidence except for a small region near the leading edge where there may be a laminar separation bubble. The variation of drag coefficient with incidence is shown in Fig. 21. There is a progressive decrease of the minimum-drag coefficient and an increase of the incidence at which the drag rise occurs as the Reynolds number is increased. This is a typical variation with Reynolds number as can be seen by comparison with Fig. 3b of Ref. 8. The variation of pitching-moment coefficient with incidence is shown in Fig. 22 and there is again a consistent variation with Reynolds number. Comparing the mean slopes of the lift and pitching-moment coefficient curves at 140 ft/sec (42·7 m/s) over the unstalled incidence range the aerodynamic centre is 5·8 per cent of the mean chord forward of the mean quarter-chord point.

5. *Wake and Boundary-Layer Traverse and Flow Visualisation Results.*

5.1. *Wake-Traverse Results*

The results of the wake traverses on the tailplane pivot line are shown in Fig. 23. Below the stall the shape of the curves is determined by two factors: the fuselage boundary layer (*see* also Section 5.2) and the spanwise static-pressure gradient caused by the potential flow field round the wing-body combination. When the wing stalls there is not a uniform reduction in dynamic pressure across the rake span, presumably because firstly the boundary of the wing wake is curved in transverse planes and secondly the wing stalls progressively, the flow separation on the top surface moving inboard from the tip as incidence is increased. The effect of changes in the wing planform on the wake, as measured at the low tailplane position, can be seen by comparing Figs. 23a, c and d; in particular, because the trailing vortex sheet from the wing-body combination is much changed in the inboard region, extending the wing planform has a large effect at high incidence. The greater dynamic pressure obtainable in the high tailplane position can be seen by comparing Figs. 23b and c.

In order to separate the factors contributing to the effectiveness of the tailplane a mean dynamic pressure at the tailplane was determined from the wake-traverse results. As the tailplane was tapered it was thought that taking a simple mean of the dynamic pressure measured at a given incidence was insufficiently accurate. Instead a mean was calculated assuming that the tailplane loading was proportional to the local chord (which is equivalent to assuming a constant sectional lift coefficient). The mean was taken across the wetted area only. The measured dynamic pressure was multiplied by the chord and this integrated across the tailplane span before finally dividing by the relevant area. The results are shown in Fig. 24 for the four cases tested.

5.2. *Boundary-Layer Traverse Results.*

Boundary-layer profiles, obtained at the low tailplane position over a range of wing incidence for the clean wing with and without high-lift devices, are shown in Figs. 25 and 26. Comparison with the profile typically found for flat-plate boundary layers suggests that below the stall the profiles are of the type found in an adverse pressure gradient approaching separation. Above the stall the form of the profile changes completely, presumably because the local free stream has a much reduced dynamic head, and the profile is similar to a flat-plate boundary-layer profile.

The profiles obtained with the clean wing with high-lift devices, below the stall, appear to be made up of two parts. An established boundary layer, which has travelled some distance down the body, to which has been added some higher energy air near the body surface. This higher energy air probably comes from air channelled through the gap which exists between the body and the inboard end of the flap.

5.3. *Flow Visualisation Results.*

Some of the surface flow patterns obtained with the clean wing and the tailplane in the low position are shown in Fig. 27. At all three incidences there is no sign of any extensive region of separated flow near the tailplane. The form of the tailplane-body junction flow is similar to that at the wing-body junction although the details of the flow are not so easily visible at the tailplane. The vortices leaving the wing-body junction can be seen to cause cross flow on the body immediately adjacent to the wing but they are sufficiently weak for them to have little effect on the surface flow pattern at the tail. The flow always remains attached to the undersurface of the moderately unswept tail of the fuselage.

The surface flow patterns obtained for the tailplane were not photographed as the quality of the results was poor. Some comments on the results have been made in Section 4.4.

6. *Tailplane Effectiveness.*

6.1. *The Factors Determining Tailplane Effectiveness.*

Considering the factors listed in the introduction in more detail:

The effects of the wing wake and the fuselage boundary layer on the velocity field at the tailplane may be conveniently grouped together. A mean dynamic pressure at the tailplane may be defined, $(q_t/q_o)_M$, weighted according to the load distribution on the tailplane.

The interference effect of the fuselage on the tailplane lift distribution is here considered in terms of the interference factor F, defined as:

$$F = \frac{\text{Lift of wetted tailplane area and body between the tailplane halves}}{\text{Lift of total area of tailplane in a uniform stream having the same mean dynamic pressure}}. \quad (2)$$

This definition of an interference factor differs slightly from that used in Ref. 2 where the factor arises from a theoretical method used to estimate the lift of a combination of a surface and an infinite body. The above definition (2) has been used so as to include the possible effect of separations caused by placing the tailplane on the large body of the present tests in addition to the modification of the tailplane lift distribution and the carry over of lift onto the body.

As no direct measurements have been made of the downwash, the fourth factor is considered in terms of an effective downwash ε, which is defined as the intersection, on a graph of pitching moment against tail setting, of the no-tailplane curve with the curve obtained at a given wing incidence for a range of tailplane setting. Neglecting the contribution to pitching moment of the tailplane drag we may assume at these points of intersection the tailplane lift will be zero and hence the incidence of the tailplane zero-lift line relative to the free-stream direction will be equal to the mean downwash of the flow, sampled by the tailplane, due to the vortex sheet from the wing-body combination. Many attempts have been made to predict the mean downwash at the tailplane, either by a completely theoretical method involving the prediction of the trailing vortex sheet shape and position and the distribution of downwash about it and then taking a mean value at the tailplane weighted according to the tailplane loading, or by measurements of the flow direction in the plane of operation of the tailplane and then taking a weighted mean value. Silverstein and Katzoff[10], Priestly[11], DeYoung and Barling[12] and Decker[13] have reviewed existing work, formulated prediction methods and compared their methods with the effective downwash where this is known. The best accuracy of prediction that has been obtained is of the order of one degree. If a careful survey of the flow direction at the tail were made, combined with an accurate knowledge of the tailplane loading, it should be possible to improve upon the present calculation methods. There is even greater room for improvement in the prediction of the wake produced by wing-body combinations at high lift. To give an idea of the sensitivity of pitching moment to the accuracy of prediction of downwash, the accuracy of the present moment measurements ($\pm 0{\cdot}003$ on C_m) is equivalent to prediction of downwash to $0{\cdot}05°$ which is beyond anything likely to be achieved by theoretical prediction methods.

In order to isolate the tailplane-body interference, the effective downwash ε, determined in the manner described above, and the measured dynamic pressure have been used throughout the present analysis. A consequence of using the downwash defined in this way is that it is assumed constant for a range of tail

setting at constant wing incidence. In fact this may not be so for a swept tailplane which samples a different part of the downwash field as the tail setting is changed. In terms of the factors defined above the effective contribution of the tailplane can be derived as follows.

If the lift-curve slope of the tailplane measured in a separate test is a_t then the effective lift-curve slope of the tailplane mounted on the model will be a_{t_E} where:

$$a_{t_E} = \left(\frac{q_t}{q_o}\right) F\, a_t \tag{3}$$

and a mean incidence of the tailplane may be defined using the effective downwash ε:

$$\alpha_t = \alpha_w - i_w + i_t - \varepsilon\,. \tag{4}$$

Thus the lift of the tailplane will be:

$$C_{L_t} = a_{t_E}\,\alpha_t\,. \tag{5}$$

Again neglecting the contribution of the tailplane drag to the overall forces and moments (which is a reasonable assumption below the stalling incidence of the tailplane) the overall effectiveness of the tailplane can be considered in terms of the contribution of the tailplane lift to the overall lift-curve slope of the whole model, which will be:

$$\frac{d\,C_{L_t}}{d\,\alpha_w} = \alpha_t \frac{d\,a_{t_E}}{d\,\alpha_w} + a_{t_E}\left(1 - \frac{d\,\varepsilon}{d\,\alpha_w}\right). \tag{6}$$

The first term is usually neglected in stability analysis but it can become appreciable near the stall where $(q_t/q_o)_M$ is changing rapidly. The discussion which follows in Sections 6.2 and 6.3 is concerned with the effective tailplane lift-curve slope and the efficiency is defined as the ratio of this slope to the tailplane lift-curve slope measured in a separate test. The problem of the downwash field at the tailplane is not considered here except where it is relevant to the tailplane efficiency.

6.2. *Tailplane Efficiency of the Present Tests.*

The effective downwash was first calculated by the method described in Section 6.1. The results are plotted in Fig. 28. The advantage of a high tailplane position can be seen as a reduction in the slope of downwash with wing incidence, $(d\varepsilon/d\alpha_w)$, which will therefore increase the tailplane contribution to the overall lift-curve slope (equation (6)). From the same graph used to obtain the effective downwash the partial derivative of pitching moment with respect to the tail setting at constant wing incidence, $(\partial C_m/\partial i_t)_{\alpha_w}$, was measured. The mean slopes at a given wing incidence are plotted in Fig. 29.

The effective downwash obtained above was used to resolve the differences in lift, drag and pitching-moment coefficients, measured with and without the tailplane in position, to obtain the effective tailplane characteristics. The relevant equations are derived in the Appendix. The results are shown in Fig. 30 and Fig. 31 for the clean wing without high-lift devices and for the clean wing with high-lift devices and the extended wing respectively. In each case the derived lift and drag coefficients are plotted against the effective tailplane incidence. The non-linearity of the tailplane lift curve over the unstalled incidence range which was found in the separate railplane test (Fig. 20) is apparent in the derived lift curves. The best straight line has been drawn through the lift coefficient *versus* tailplane-incidence results over the incidence range $\pm 10°$. The values of the slopes obtained are tabulated below, and plotted in Fig. 32b.

Model arrangement		a_{t_E}	Efficiency	$\left(\frac{q_t}{q_o}\right)_M$ at	Interference
Wing	Tail	per degree	$\frac{a_{t_E}}{a_t}$	low incidence	$F = \frac{a_{t_E}}{a_t\left(\frac{q_t}{q_o}\right)_M}$
Clean	High	0·0652	1·035	1·030	1·005
	Mid	0·0632	1·003	1·000*	1·003
	Low	0·0570	0·905	0·880	1·028
Clean with flaps with droop	Low	0·0533	0·846	0·882	0·959
Extended planform	High	0·0645	1·024	1·030	0·994
	Low	0·0564	0·895	0·891	1·004

*Estimated value.

Also tabulated here are the tailplane efficiency (as given by the ratio of the lift-curve slopes with the tailplane mounted on the model and in the separate tailplane test), the mean value of $(q_t/q_o)_M$ over a wing incidence range of 0° to 10°, and the derived interference factor F, obtained by dividing the efficiency by the mean dynamic pressure. It has been assumed that changing the wing planform has little effect on the mean dynamic pressure at the high tailplane position. The accuracy of the determination of the mean dynamic pressure for the high and mid tailplane positions should be good as there is little variation of dynamic pressure across the span, so that the mean value will be insensitive to the tailplane loading assumed in the weighting of the local values of dynamic pressure. As might be expected there is negligible interference for these two tailplane positions which suggests that the tailplane efficiency for similar tailplane arrangements may be determined by a simple wake traverse on the tailplane pivot line.

The problem is more complicated for the low tailplane position. The calculation of the mean dynamic pressure for the wetted area of the tailplane using a constant sectional lift-coefficient weighting implies that when this mean dynamic pressure is used to calculate the interference factor it is implicitly assumed that both this mean dynamic pressure and the constant sectional lift coefficient operate on the part of the tailplane covered by the body. The interference factor may then be thought of as the way in which the tailplane and body sectional lift coefficient and mean dynamic pressure are altered from these constant values because of the interference. The overall experimental accuracy of the determination of these interference factors is about $\pm 0{\cdot}5$ per cent. To this accuracy there is a gain of 3 per cent for the clean wing, no net interference for the extended wing and a loss of 4 per cent for the clean wing with high-lift devices. These values of the interference factor confirm the flow visualisation result that there is no major separation at the tailplane-body junction. The interference becomes progressively more unfavourable as the inboard part of the wing, which has a major influence on the tailplane downwash field, is modified from the straight tapered form. As can be seen from Fig. 28 the effective downwash at a given wing incidence increases, as the wing is modified, for the three low tailplane cases. A large amount of this increase will occur at the wing root so that the tailplane-body junction flow may be considerably changed. This conclusion is reinforced by calculations made by DeYoung and Barling[12]. The downwash they computed in the wing root region was found to be critically dependent upon the span loading in this region. The contribution of the body to the downwash at the tailplane could only be considered independently of the wing contribution if the body diameter was small compared with the body length and wing span. The existing method of calculating the tailplane-body interference, due to Weber, Kirby and Kettle[14], is limited to the flow over a lifting surface mid mounted on an infinite cylindrical body. As the tailplane of the present model was mounted on a sharply-tapered, upswept body of non-circular cross section it was not considered that this calculation method would produce any meaningful results.

The derived drag coefficient *versus* tailplane incidence curves shown in Figs. 30 and 31 have too much scatter for it to be worthwhile attempting a similar analysis to that performed above for lift. The shape

of the drag-coefficient curves and the minimum drag coefficients agree well with those obtained in the separate tailplane test (Fig. 21).

Some calculations have been made (using the equations derived in the Appendix) to predict the model characteristics when fitted with a tailplane by starting from the model forces and moments measured without a tailplane and adding the contribution of the tailplane as determined from the separate tailplane test and the wake-traverse measurements. Unfortunately it was necessary to use the derived downwash in this process so that the calculations were not independent of the original measurements with a tailplane mounted on the model and hence the results are of limited value. As the downwash was determined only at the tailplane zero-lift angle to an accuracy of about $\pm 0{\cdot}2°$ there was considerable scope for error in the derived characteristics. In fact the errors were rarely more than the equivalent of $0{\cdot}25°$ on the value of the downwash.

6.3. *Other Measurements of Tailplane Efficiency.*

A rough correlation between tailplane efficiency (as measured by the ratio a_{t_E}/a_t) and the size of the body relative to the tailplane, when it is mounted on the body, has been made by Neely and Griner, (Fig. 28 of Ref. 2). The results of the present tests fall near this curve even though the body of the model tapers sharply to the relatively low value of the ratio of the body width at the tailplane to the tailplane span. However the scatter about the correlation of Ref. 2 is large. Neely and Griner[2] make little mention of the variation of tailplane efficiency with tail height other than to suggest a value of 0·90 to 0·95 for the tailplane immediately adjacent to the body and 1·00 for the tailplane well removed from the body. Much of Ref. 2 is concerned with the prediction of the downwash field for different tail heights.

The results of Kettle [3] for a range of body sizes, tailplane arms, and heights, have been analysed to find the variation of tail efficiency with body size and tailplane position. A simple measure of tailplane efficiency can be obtained by considering the mean value of the partial derivative $(\partial C_m/\partial i_t)_{\alpha_w}$ for a range of wing incidence. This was obtained from a graph of pitching moment against tailplane setting for the various wing-body-tail arrangements of Ref. 3. As can be seen from equation (A.3) of the Appendix the effective lift-curve slope is given by: $-S\bar{c}/S_t\, l_t\, (\partial C_m/\partial i_t)_{\alpha_w}$ to a first approximation; (the ratio $S\bar{c}/S_t\, l_t$ is the reciprocal of the tail volume ratio $\bar{V}$). The mean value of this quantity over the incidence range of the tests is plotted in Fig. 33a against h_t/l_t, the ratio of the tailplane height to its moment arm. The results show a definite fall in tailplane efficiency with decrease in tailplane height but no consistent effect of body size emerges, however the scatter resulting from the crude calculation method is sufficiently large to conceal an appreciable effect of body size. For the purposes of comparison the results of the present measurements have been analysed and are plotted in Fig. 32a. There is a similar trend with decrease in tailplane height. The differences are probably accounted for by the fact that the model of Ref. 3 has a higher aspect-ratio tailplane (4.7) than the present model (4) and a body with curvature at the tailplane-body junction as opposed to the straight taper of the body of the present model so that flow separation may occur in the former case.

The method outlined in Section 6.2 was used to derive the effective tailplane characteristics by means of the equations derived in the Appendix. The effective tailplane lift-curve slopes, obtained by putting the best straight line through the values of tailplane lift derived in this manner, are plotted against the ratio h_t/l_t in Fig. 33b. Again a decrease of tailplane efficiency is apparent as the tailplane height is reduced but, in addition, a definite effect of body size emerges with the efficiency falling as the body size is increased. Unfortunately no separate tailplane test was made, as the investigations of Ref. 3 were not primarily concerned with tailplane performance, so it was not possible to obtain an absolute measure of tail efficiency.

7. *Conclusions.*

The tailplane effectiveness of an airbus-type of aircraft model was investigated with the wing clean, with high-lift devices deflected and with the planform of the wing extended in the root region. The contributions of the tailplane to the overall lift, drag, and pitching moment of the model were derived from measurements with and without the tailplane in position. The tailplane characteristics obtained were

compared with those measured in a separate test of the tailplane alone and a measure of the tailplane efficiency was thus derived. The component of this efficiency due to the effective dynamic pressure at the tailplane was determined by a series of wake traverses on the tailplane pivot line and boundary-layer measurements on the body surface.

From these results it was concluded that:

(1) For tailplane mounting positions away from the body the effective dynamic pressure accounted for nearly all the change in tailplane characteristics and the interference involved in mounting the tailplane was there fore negligible.

(2) For tailplane mounting positions on the body there was a small interference effect (less than 5 per cent of the tailplane lift) of the body on the tailplane lift.

(3) The body interference was a function of the downwash field at the tailplane and became progressively worse as the inboard section of the wing was modified from the clean wing to the extended planform wing and then to the clean wing with high-lift devices deflected.

LIST OF SYMBOLS

A	Wing aspect ratio
A_t	Tailplane aspect ratio
a_t	Tailplane lift-curve slope measured in separate tailplane tests
a_{t_E}	Effective tailplane lift-curve slope when the tailplane is mounted on the model
b	Wing gross span
b_t	Tailplane gross span
C_D	Drag coefficient of complete model with tailplane
C_{D_t}	Drag coefficient of tailplane
$C_{D_{wB}}$	Drag coefficient of wing-body combination without tailplane
ΔC_D	$C_D - C_{D_{wB}}$
C_L	Lift coefficient of complete model with tailplane
C_{L_t}	Lift coefficient of tailplane
$C_{L_{wB}}$	Lift coefficient of wing-body combination without tailplane
ΔC_L	$C_L - C_{L_{wB}}$
C_m	Pitching-moment coefficient of complete model with tailplane as defined in Section 3.1
C_{m_t}	Pitching-moment coefficient of tailplane
$C_{m_{wB}}$	Pitching-moment coefficient of wing-body combination without tailplane
ΔC_m	$C_m - C_{m_{wB}}$
δC_m	Correction applied to pitching moment to account for the wind-tunnel constraint at the tailplane
$\bar{c}$	Mean chord of wing
$\bar{c}_t$	Mean chord of tailplane
F	Tailplane interference factor
H	Boundary-layer shape factor
h_t	Tailplane height relative to the wing quarter-chord point as measured in body axes
h'	Tailplane height as measured in wind axes at the tailplane $h' = l_t \sin(\alpha_w - i_w - \varepsilon) - h_t \cos(\alpha_w - i_w - \varepsilon)$
l_t	Tailplane arm relative to the wing quarter-chord point as measured in body axes
l'	Tailplane arm as measured in wind axes at the tailplane $l' = l_t \cos(\alpha_w - i_w - \varepsilon) + h_t \sin(\alpha_w - i_w - \varepsilon)$
q_o	Dynamic pressure at the balance centre corrected for wind-tunnel blockage
q_t	Dynamic pressure at some point on the tailplane pivot axis
S	Gross wing area
S_t	Gross tailplane area

U Velocity at some point in the boundary layer measured at the tailplane pivot position

U_o Velocity corresponding to the reference dynamic pressure q_o

U_1 Velocity at the edge of the boundary layer

$\bar{V}$ Tail volume ratio $= S_t\, l_t / S\, \bar{c}$

y Lateral co-ordinate measured from the body surface at the tailplane pivot normal to the surface

The subscript M indicates a weighted mean value

α_t Tailplane incidence; $\alpha_w - i_w + i_t - \varepsilon$

$\Delta\alpha_t$ Constraint correction to the flow direction at the tailplane

α_w Wing incidence

$\Delta\alpha_w$ Constraint correction to the flow direction at the wing

$\delta_{0\cdot995}$ The height in a boundary layer at which the velocity is 99·5 per cent of that of the local free stream U_1

δ_1 Displacement thickness of boundary layer

δ_2 Momentum thickness of boundary layer

ε Derived downwash; this is the mean value of the downwash determined from equation (4) when the tailplane has zero net lift and thus $\alpha_t = 0$

i_t Tailplane setting relative to the body axis

i_w Wing setting relative to the body axis

REFERENCES

No.	*Author(s)*	*Title, etc.*
1	F. N. Kirk	Tail efficiency. R.A.E. Technical Note Aero 1717 (A.R.C. 9519) (1946).
2	R. H. Neely and R. F. Griner..	Summary and analysis of horizontal-tail contribution to longitudinal stability of swept-wing airplanes at low speeds. NACA RM L55E23a TIL 5867 (1955).
3	D. J. Kettle	The effects of fuselage length and shape on the aerodynamic characteristics of transport aircraft of large capacity. R.A.E. work to be published.
4	D. J. Kettle and D. A. Kirby ..	Low-speed wind-tunnel tests on the effects of tailplane and nacelle position on the superstall characteristics of transport aircraft. A.R.C. R. & M. 3571 (1967).

REFERENCES—*continued*

No.	*Author(s)*	*Title, etc.*
5	D. A. Lovell	Low-speed wind-tunnel tests on the effects of tailplane height, nacelles and high-lift devices on the superstall characteristics of a model of the airbus type of aircraft. R.A.E. Technical Report 70 031 (1970).
6	D. A. Lovell	Wall corrections to longitudinal components measured on wind-tunnel models with tails. A.R.C. C.P. 1075 (1968).
7	R. L. Maltby and R. F. A. Keating	Flow visualisation in low-speed wind tunnels. Current British practice. R.A.E. Technical Note Aero 2715 (A.R.C. 22373) (1960).
8	J. E. Fitzpatrick and G. V. Foster	Static longitudinal aerodynamic characteristics of a 52° sweptback wing of aspect ratio 2·88 at Reynolds numbers from 2 000 000 to 11 000 000. NACA/TIB/1979 (A.R.C. 15279) (1948).
9	S. N. Jacobs and A. Sherman..	Airfoil section characteristics as affected by variations of the Reynolds number. NACA Report 586 (1937).
10	A. Silverstein and S. Katzoff ..	Design charts for predicting downwash angles and wake characteristics behind plain and flapped wings. NACA Report 648 (A.R.C. 3981) (1939).
11	E. Priestly	An investigation of wake and downwash behind wings and wing-body combinations without flaps or propellers. A.R.C. R. & M. 2122 (1945).
12	J. DeYoung and W. H. Barling	Prediction of downwash behind swept-wing airplanes at subsonic speed. NACA Technical Note 3346 (1955).
13	J. L. Decker	Prediction of downwash at various angles of attack for arbitrary tail locations. *Aeronautical Engineering Review*, pp. 22–27, 61, August 1956.
14	J. Weber, D. A. Kirby and D. J. Kettle ..	An extension of Multhopp's method of calculating the spanwise loading of wing-fuselage combinations. A.R.C. R. & M. 2872 (1951).

APPENDIX

A.1. *Calculation of the Tailplane Lift, Drag and Pitching-Moment Coefficients from the Difference of Measurements made with and without the Tailplane in Position.*

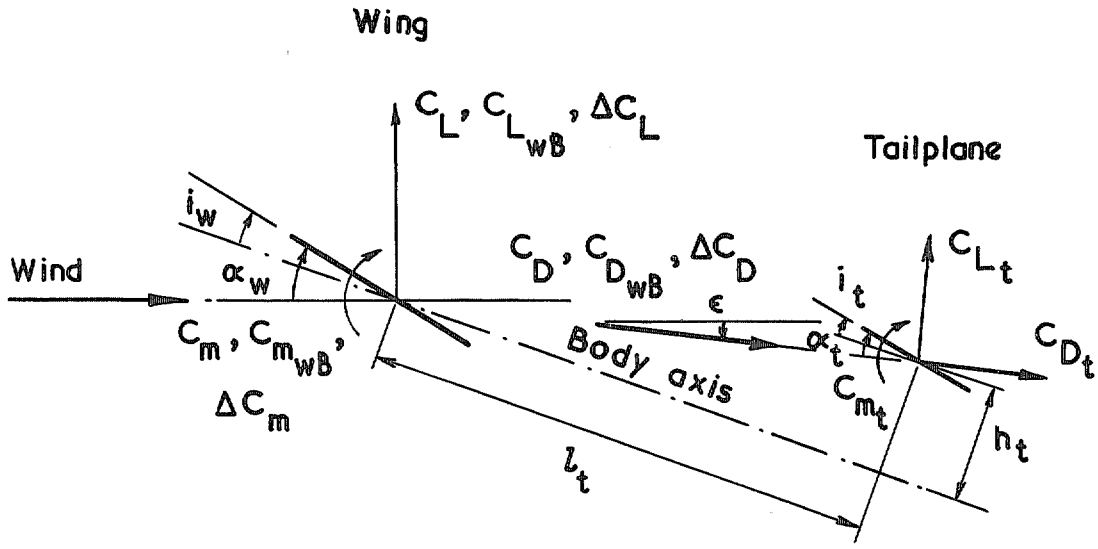

Using the notation of the above sketch, which is also defined in the list of symbols, the tailplane lift is:

$$C_{L_t} = \frac{S}{S_t}[\Delta C_L \cos\varepsilon + \Delta C_D \sin\varepsilon]. \tag{A.1}$$

Similarly for drag:

$$D_{D_t} = \frac{S}{S_t}[\Delta C_D \cos\varepsilon - \Delta C_L \sin\varepsilon] \tag{A.2}$$

and pitching moment:

$$C_{m_t} = \frac{S\bar{c}}{S_t \bar{c}_t}[\Delta C_m + l_t\{\Delta C_L \cos(\alpha_w - i_w) + \Delta C_D \sin(\alpha_w - i_w)\}$$

$$+ h_t\{\Delta C_L \sin(\alpha_w - i_w) - \Delta C_D \cos(\alpha_w - i_w)\}]. \tag{A.3}$$

Using these three quations and equation (4) the tailplane incidence, lift, drag and pitching-moment coefficients were calculated by means of simple computer programme.

A.2. *Calculation of Tailplane Contributions to the Overall Lift, Drag and Pitching-Moment Coefficients and the Derivative* $(\partial C_m/\partial i_t)\,\alpha_w$.

Using the same notation as above the overall lift will be:

$$C_L = \frac{S_t}{S}[C_{L_t}\cos\varepsilon - C_{D_t}\sin\varepsilon] + C_{L_{wB}} \tag{A.4}$$

TABLE 1

Geometric Details of Model.

Wing	
Gross area S	5·556 ft^2 (0·5162 m^2)
Gross span b	6·667 ft (2·032 m)
Standard mean chord $\bar{c}$	0·833 ft (0·254 m)
Centre-line chord	1·250 ft (0·381 m)
Aspect ratio A	8
Wing setting relative to the body axis i_w	4°
Leading-edge sweepback	27·87°
Quarter-chord sweepback	25°
Trailing-edge sweepback	15·58°
Taper ratio	0·333
Dihedral	0·79°
Flap chord	0·225 ft (0·069 m)
Droop chord (hinged on the lower surface)	12·5% of local chord
Extension fitted to the wing	
Gross area	0·599 ft^2 (0·0557 m^2)
Spanwise position of kink in trailing edge	(35·7% b) 1·190 ft (0·363 m)
Centreline chord of extended wing	1·757 ft (0·536 m)
Chord at position of kink	0·955 ft (0·291 m)
Trailing-edge sweep forward	8·53°
Fuselage	
Diameter	1·000 ft (0·305 m)
Overall length	7·347 ft (2·239 m)
Distance aft of nose of wing mean quarter-chord	3·337 ft (1·017 m)
Distance below fuselage centreline of wing mean quarter-chord	0·223 ft (0·068 m)
Tailplane	
Gross area S_t	1·621 ft^2 (0·1506 m^2)
Gross span b_t	2·547 ft (0·776 m)
Centreline chord	0·878 ft (0·268 m)
Standard mean chord $\bar{c}_t$	0·637 ft (0·194 m)
Aspect ratio A_t	4
Tailplane setting relative to the body axis i_t	
Variable range on fin	−10° to +10°
and body	−7·5° to +2·5°
Leading-edge sweepback	36·66°
Quarter-chord sweepback	33°
Trailing-edge sweepback	20·05°
Taper ratio	0·45
Dihedral	0°
Distance of mean quarter chord aft of wing mean quarter chord for all tailplane positions	3·431 ft (1·046 m)
Distance of mean quarter chord above the wing mean quarter chord for tailplane position: low	0·405 ft (0·123 m)
mid	1·153 ft (0·351 m)
high	1·903 ft (0·580 m)

TABLE 1—*continued*

Area of tailplane covered by the fuselage when the tailplane is in the low position	(17·83% S_t) 0·289 ft^2 (0·0268 m^2)
Distance of tailplane pivot line forward of mean quarter chord	0·029 ft (0·0088 m)
Fin	
Gross area	2·388 ft^2 (0·2218 m^2)
Height above fuselage centre-line	1·851 ft (0·564 m)
Chord (constant over span)	1·25 ft (0·381 m)
Leading-edge and trailing-edge sweepback	0°

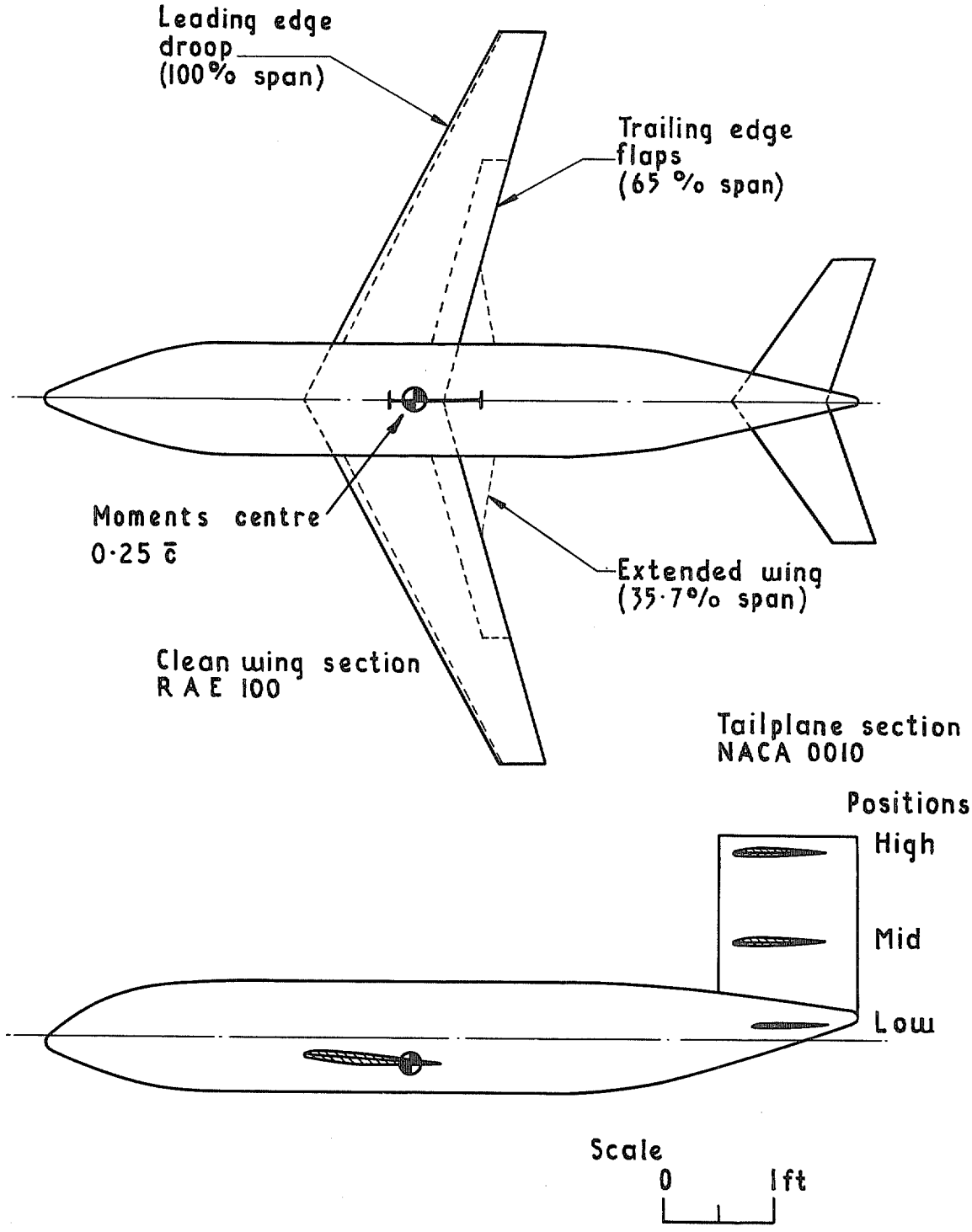

FIG. 1. General arrangement sketch of model.

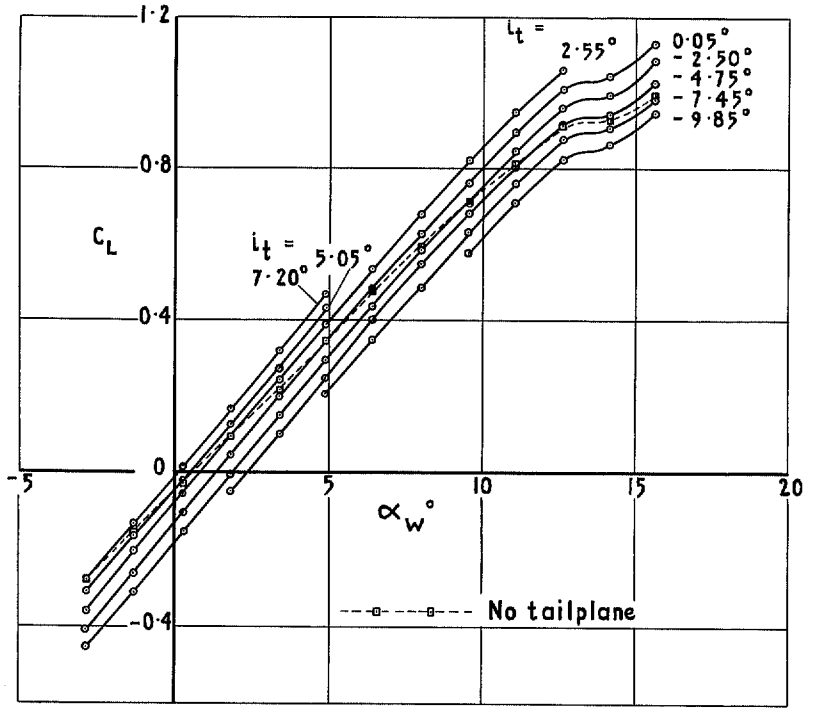

FIG. 2. C_L *vs* $\alpha_w°$ for a range of tail settings. Clean wing, high tailplane.

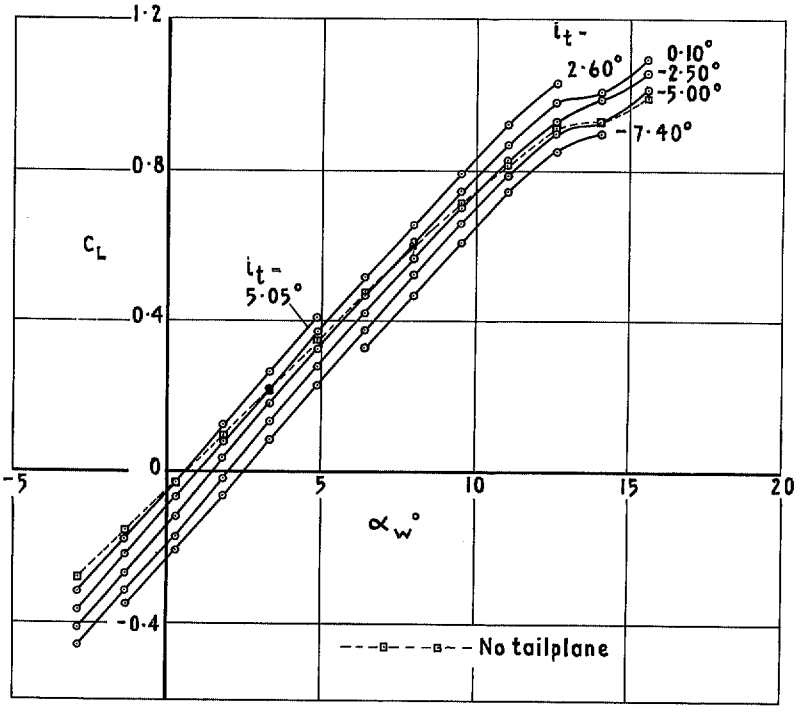

FIG. 3. C_L *vs* $\alpha_w°$ for a range of tail settings. Clean wing, mid tailplane.

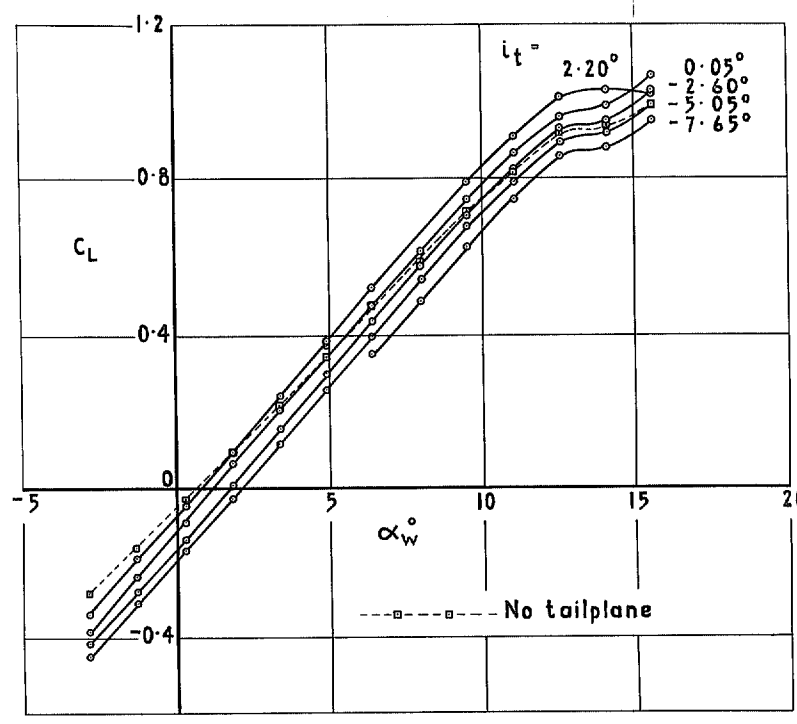

FIG. 4. C_L *vs* $\alpha_w°$ for a range of tail settings. Clean wing, low tailplane.

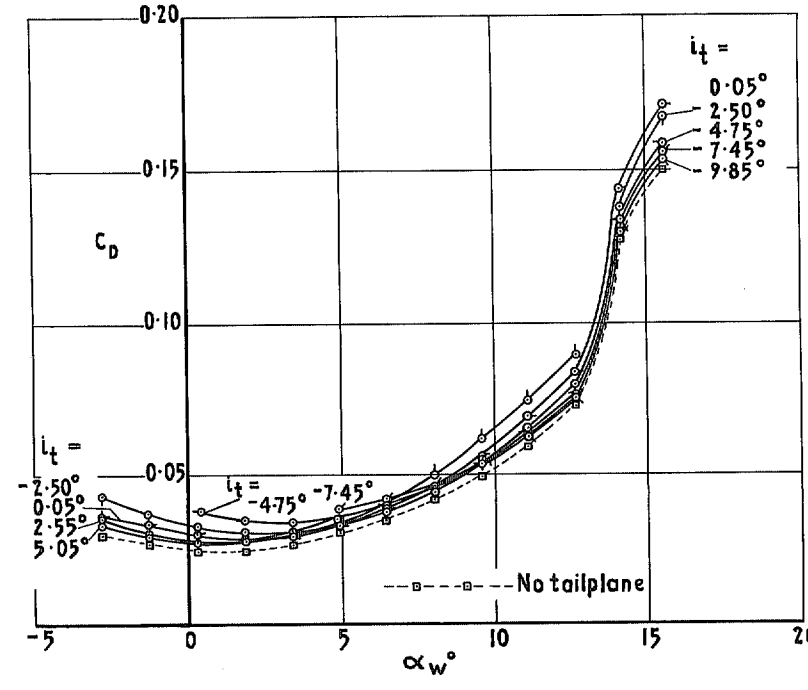

FIG. 5. C_D *vs* $\alpha_w°$ for a range of tail settings. Clean wing, high tailplane.

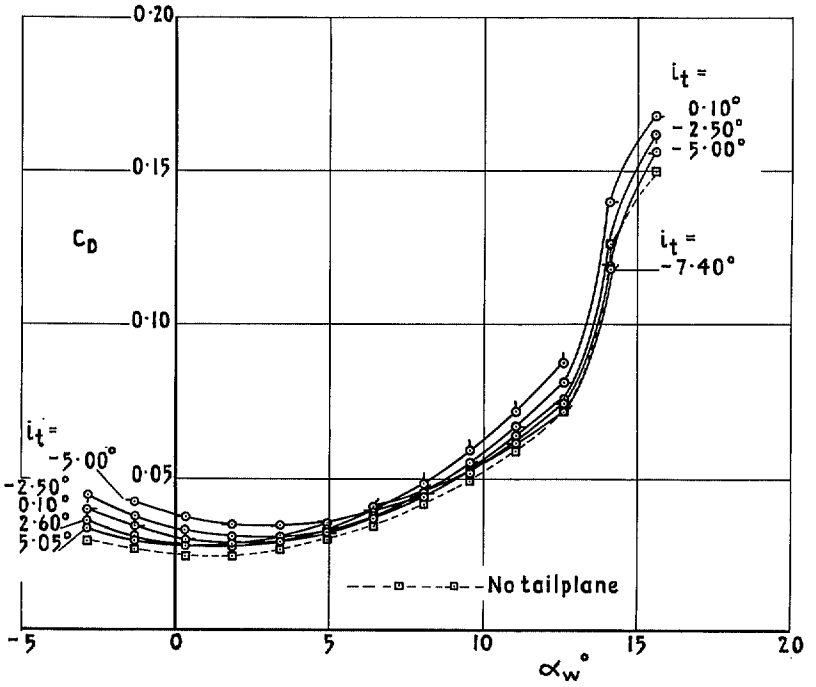

FIG. 6. C_D *vs* α_w° for a range of tail settings. Clean wing, mid tailplane.

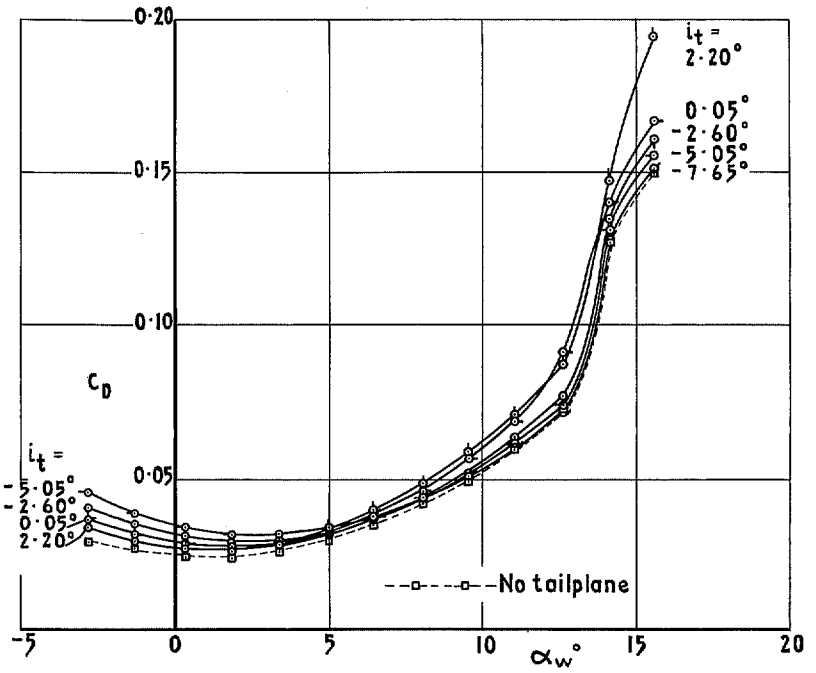

FIG. 7. C_D *vs* α_w° for a range of tail settings. Clean wing, low tailplane.

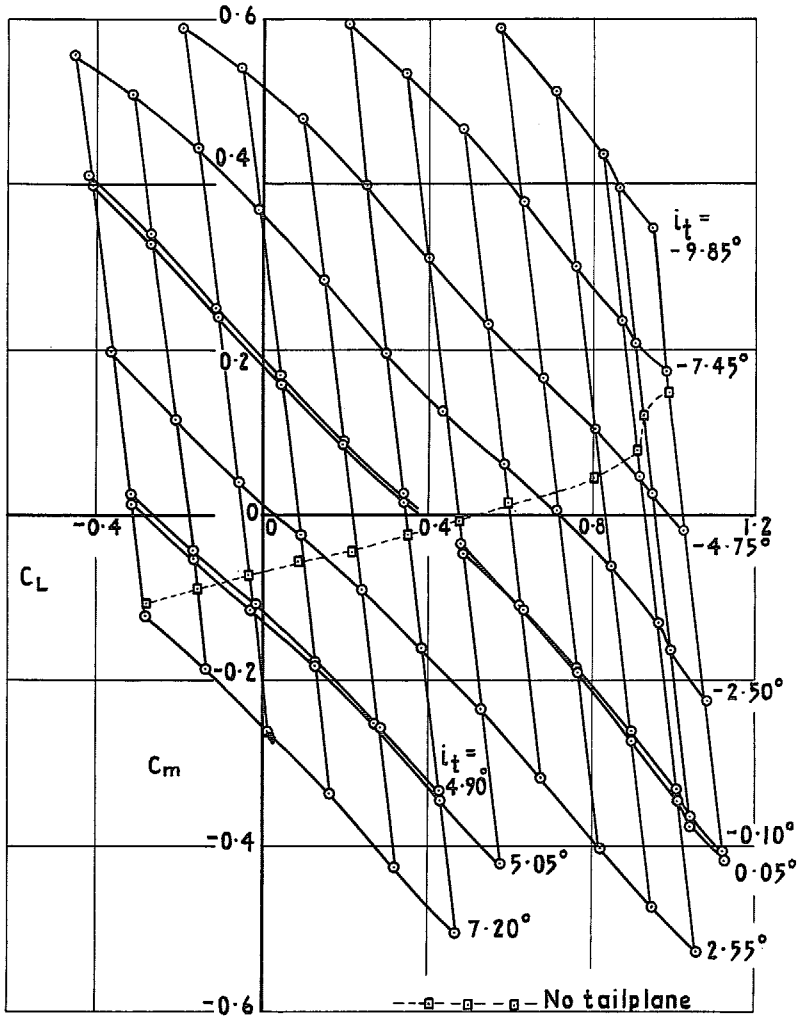

FIG. 8. C_m *vs* C_L for a range of tail settings. Clean wing, high tailplane.

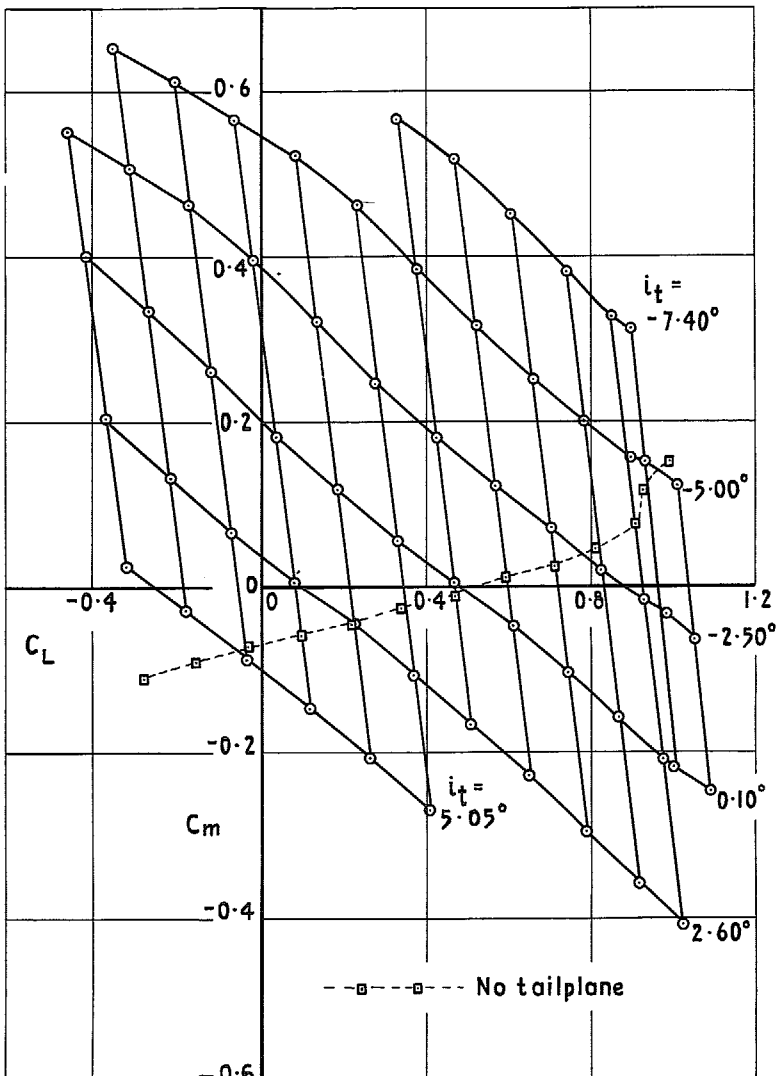

FIG. 9. C_m *vs* C_L for a range of tail settings. Clean wing, mid tailplane.

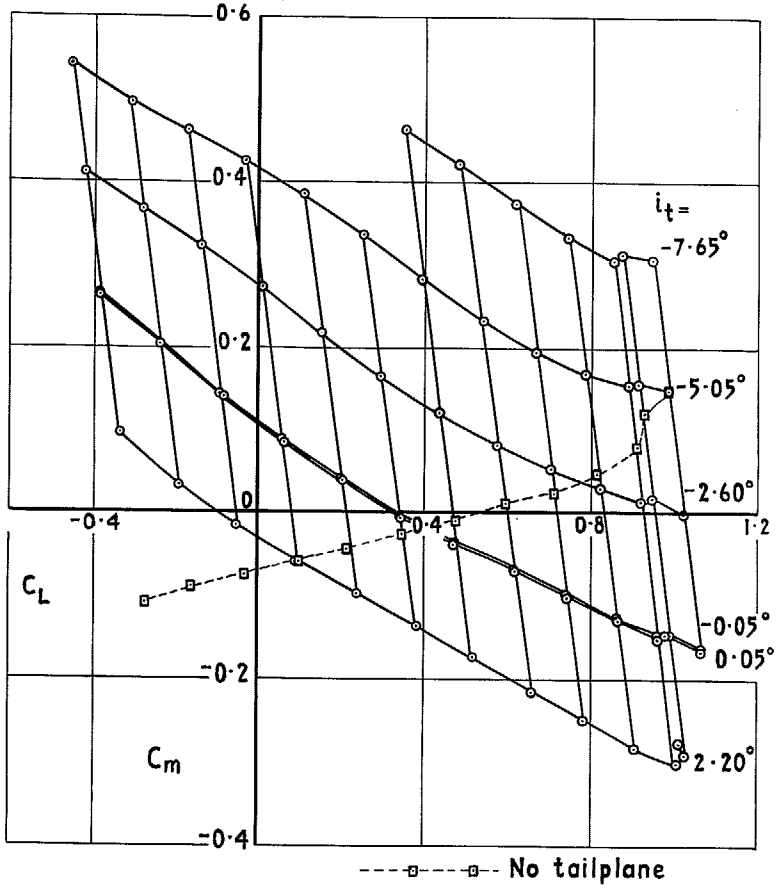

FIG. 10. C_m *vs* C_L for a range of tail settings. Clean wing, low tailplane.

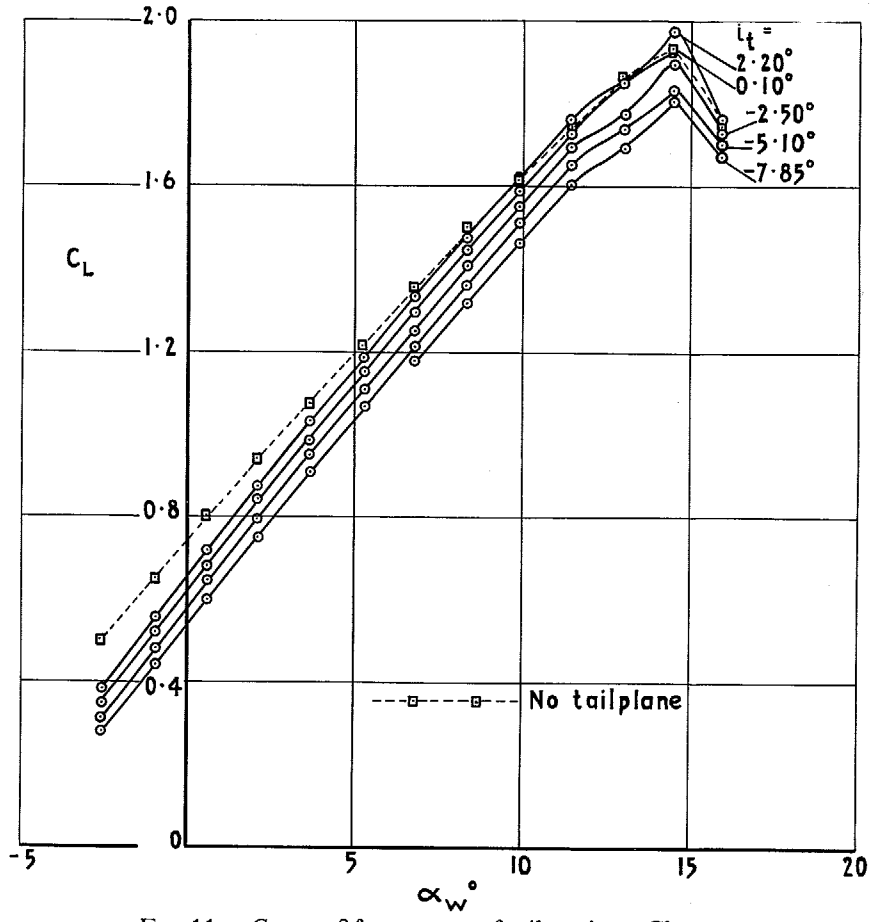

FIG. 11. C_L *vs* α_w° for a range of tail settings. Clean wing, flaps 35° and LE droop 25°, low tailplane.

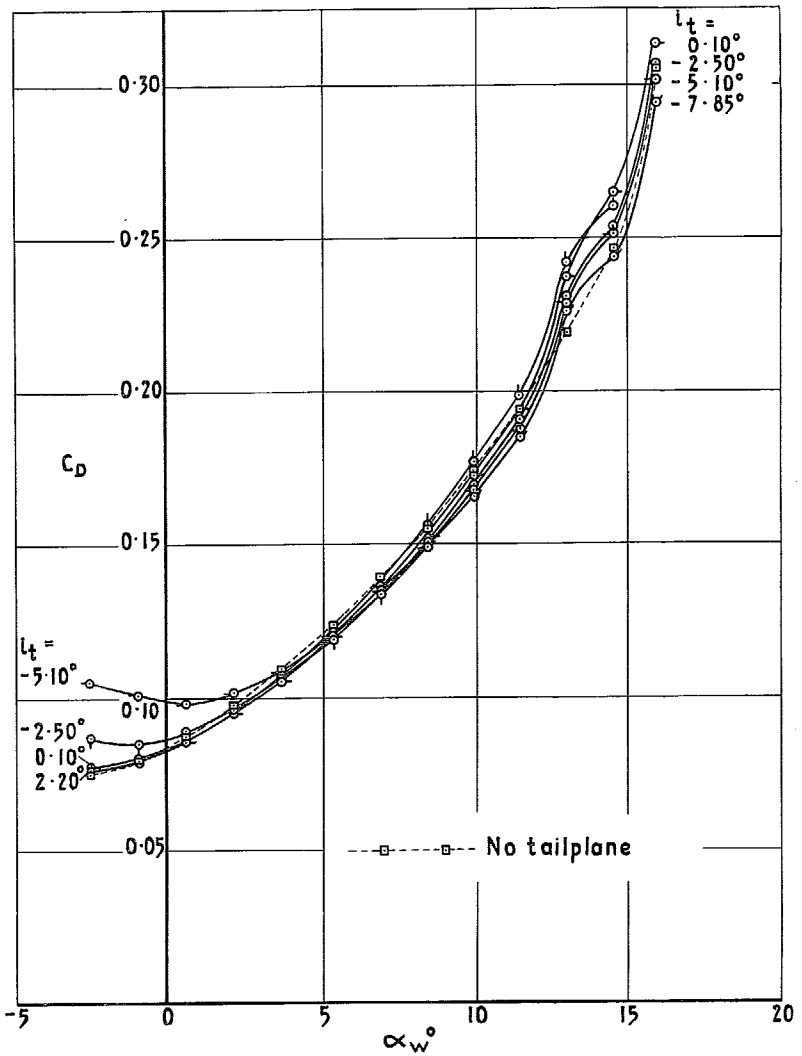

FIG. 12. C_D *vs* α_w° for a range of tail settings. Clean wing, flaps 35° and LE droop 25°, low tailplane.

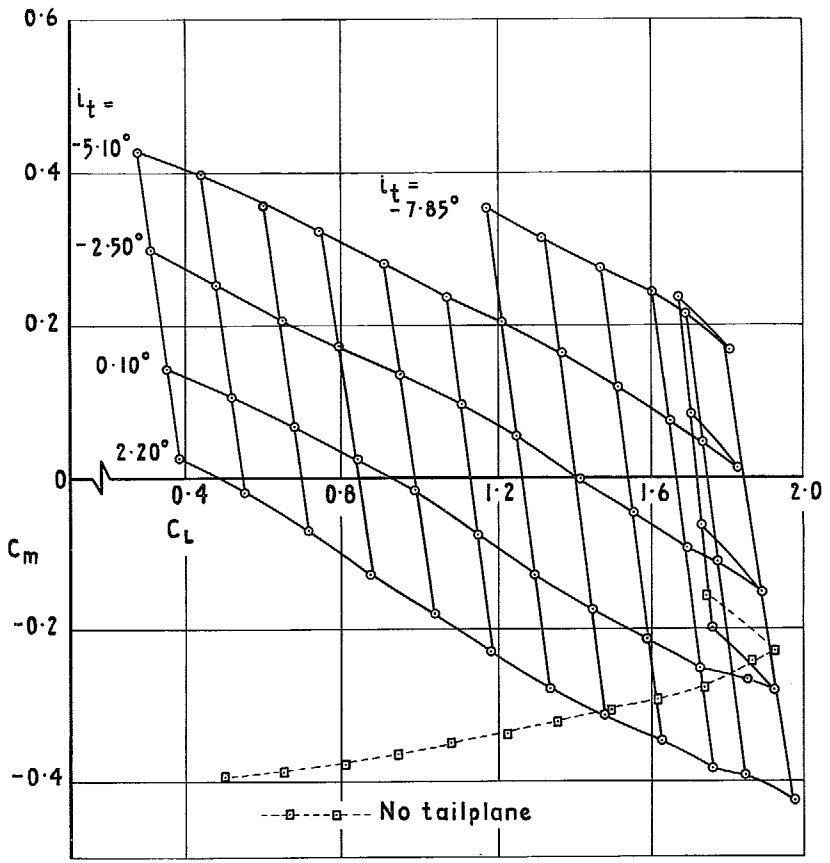

FIG. 13. C_m *vs* C_L for a range of tail settings. Clean wing, flaps 35° and LE droop 25°, low tailplane.

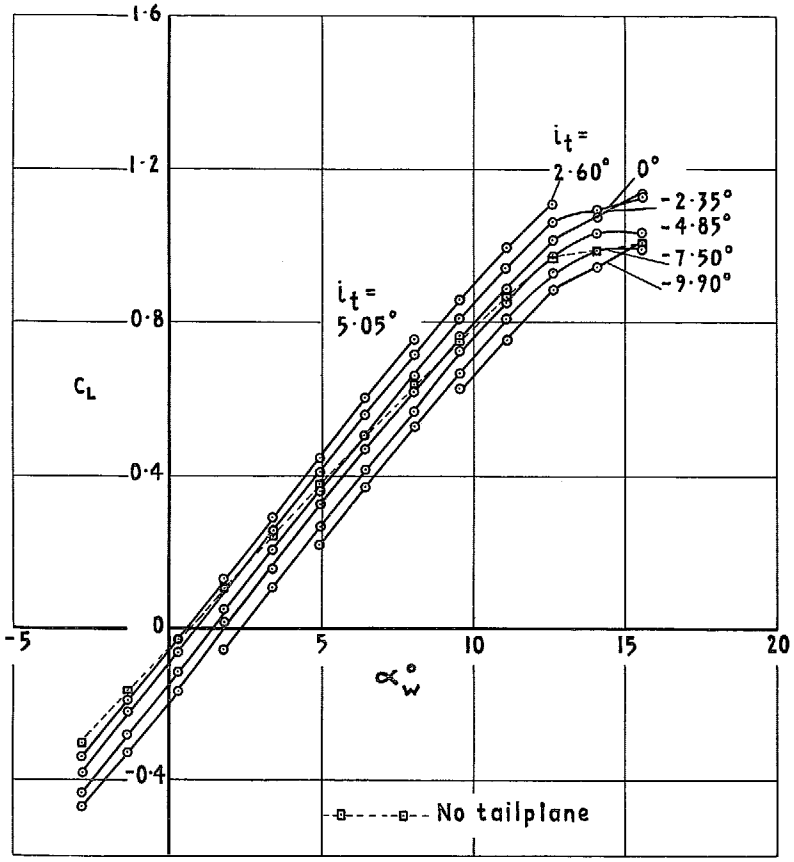

FIG. 14. C_L *vs* $\alpha_w°$ for a range of tail settings.
Extended wing, high tailplane.

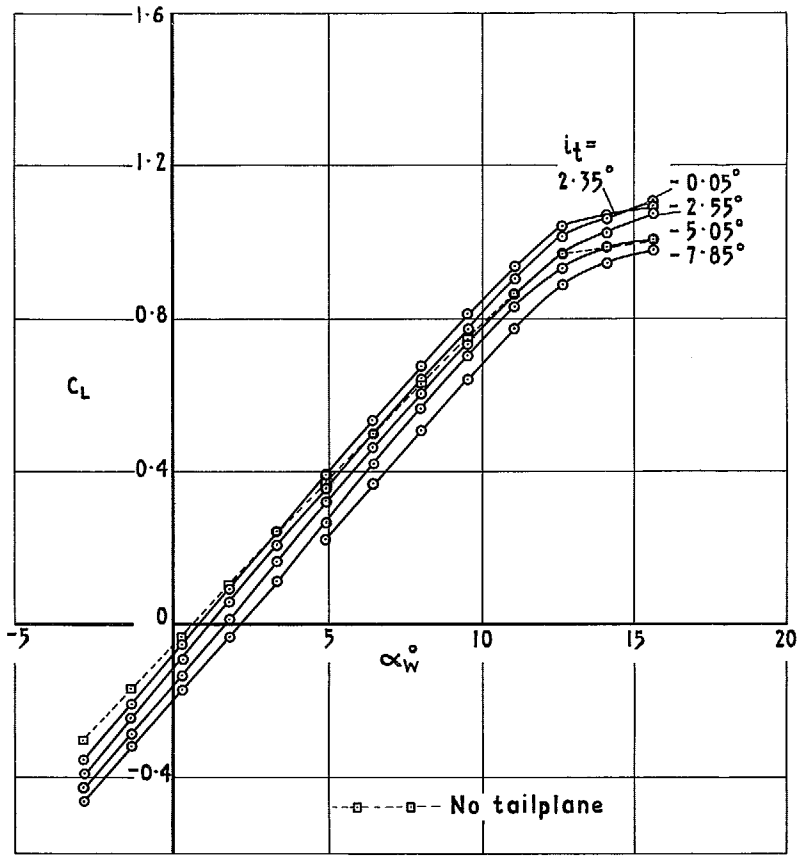

FIG. 15. C_L *vs* $\alpha_w°$ for a range of tail settings.
Extended wing, low tailplane.

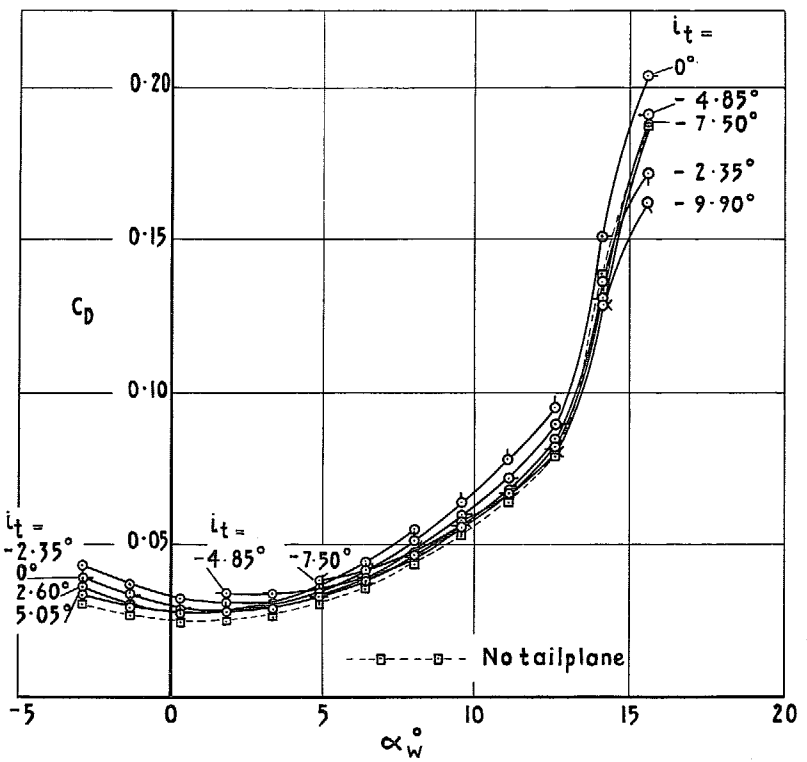

FIG. 16. C_D *vs* α_w° for a range of tail settings.
Extended wing, high tailplane.

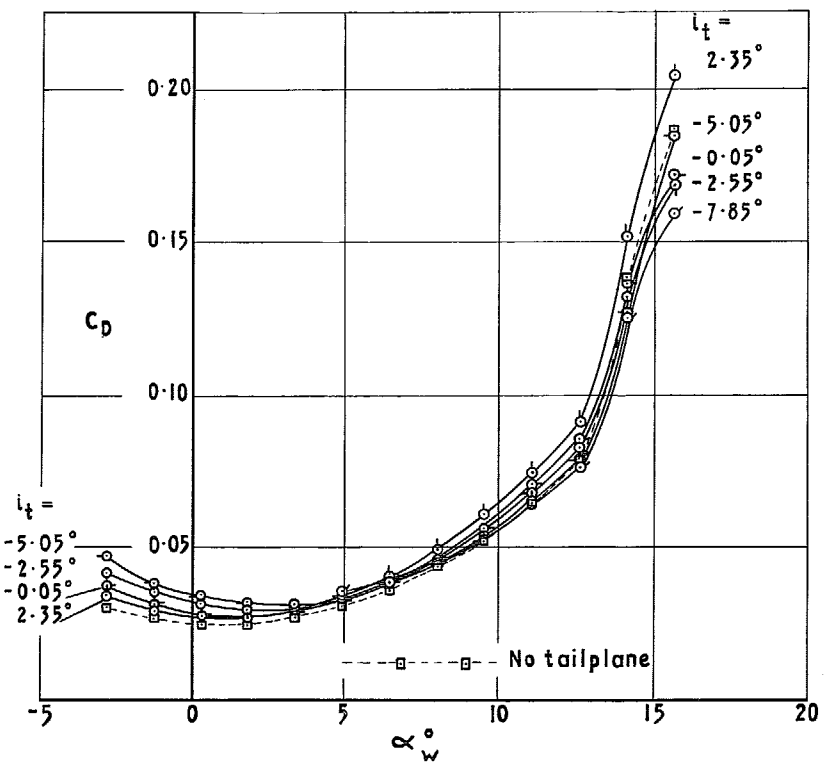

FIG. 17. C_D *vs* α_w° for a range of tail settings.
Extended wing, low tailplane.

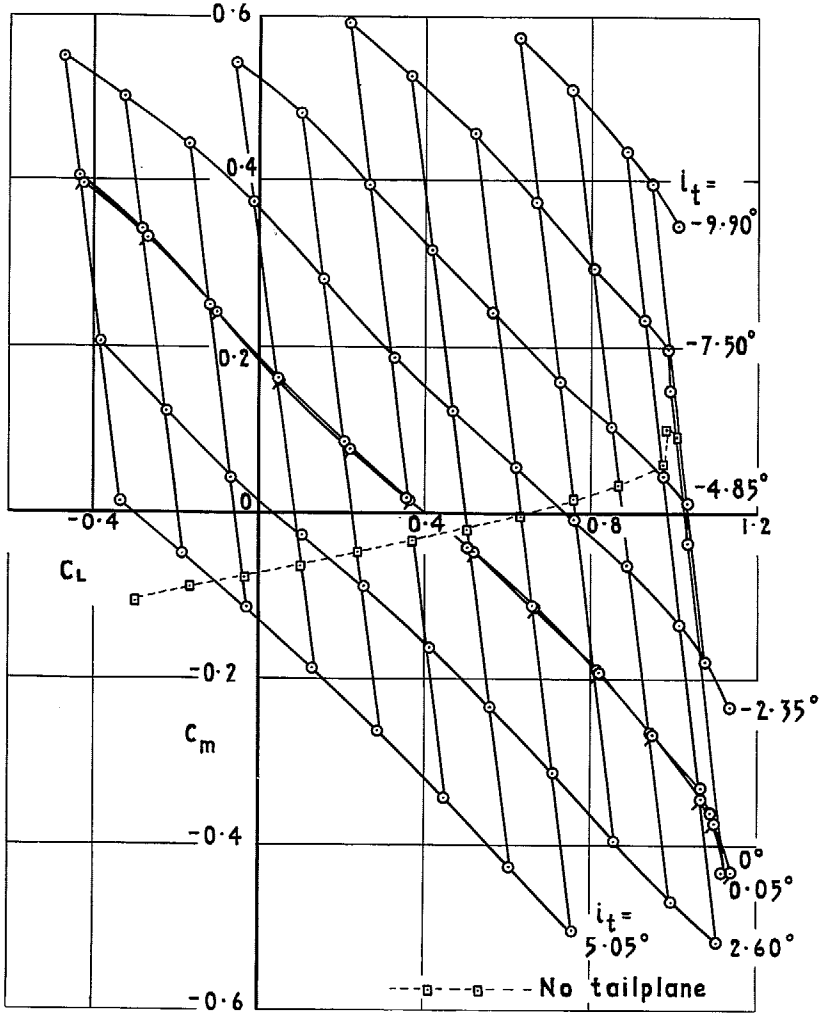

FIG. 18. C_m *vs* C_L for a range of tail settings. Extended wing, high tailplane.

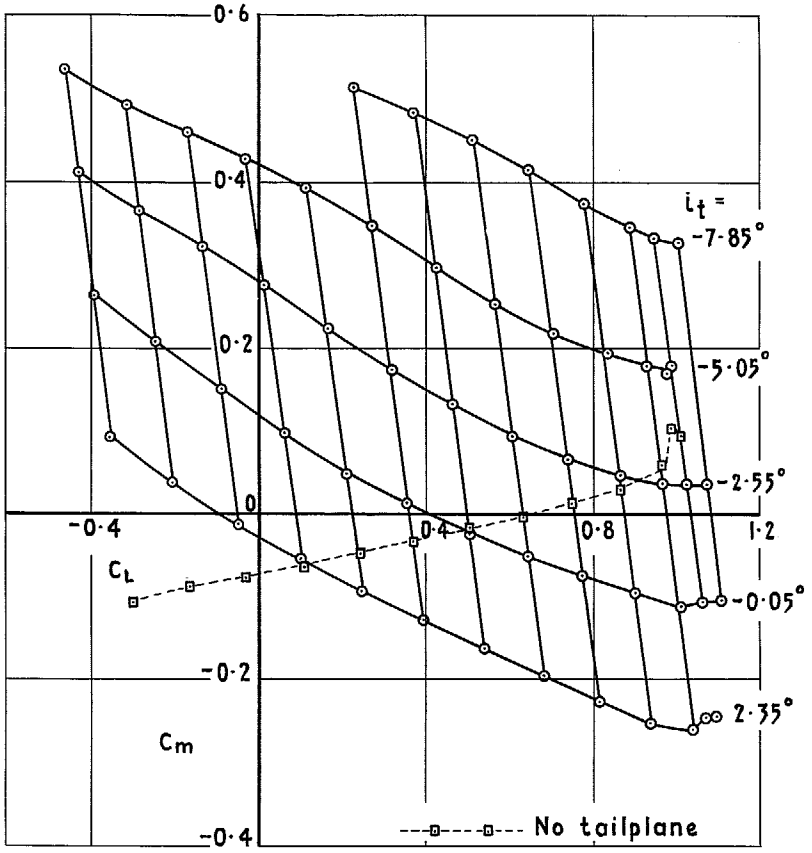

FIG. 19. C_m *vs* C_L for a range of tail settings. Extended wing, low tailplane.

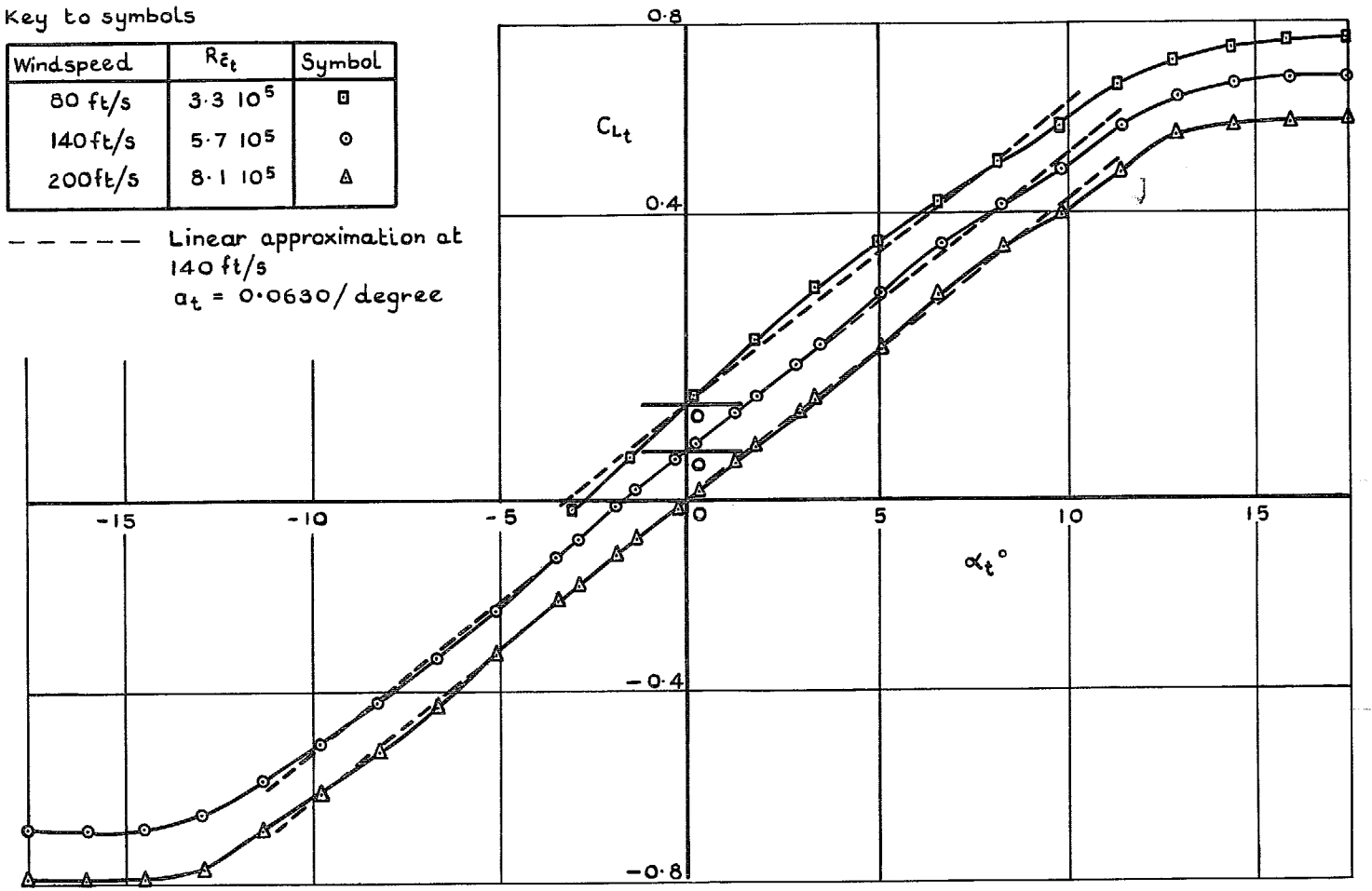

FIG. 20. C_{L_t} *vs* $\alpha_t°$. Separate test of tailplane for three windspeeds.

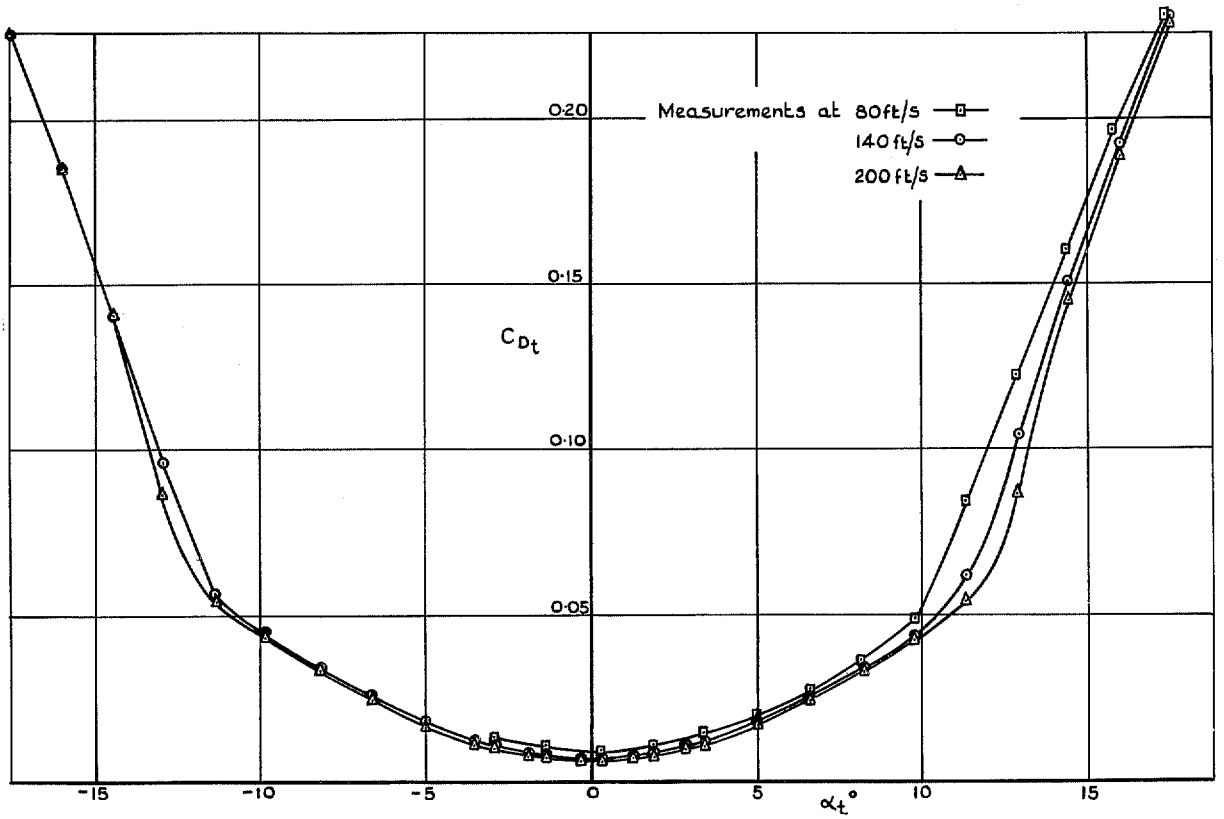

FIG. 21. C_{D_t} *vs* $\alpha_t°$. Separate test of tailplane for three windspeeds.

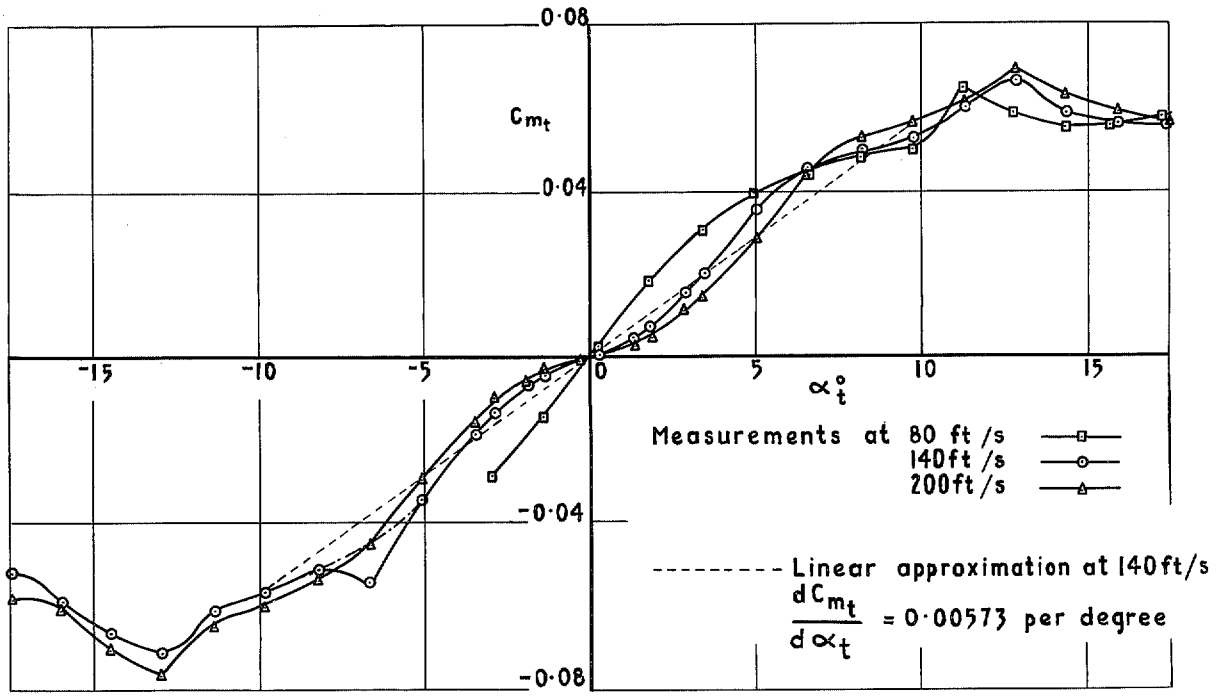

FIG. 22. C_{m_t} *vs* α_t. Separate test of tailplane for three windspeeds.

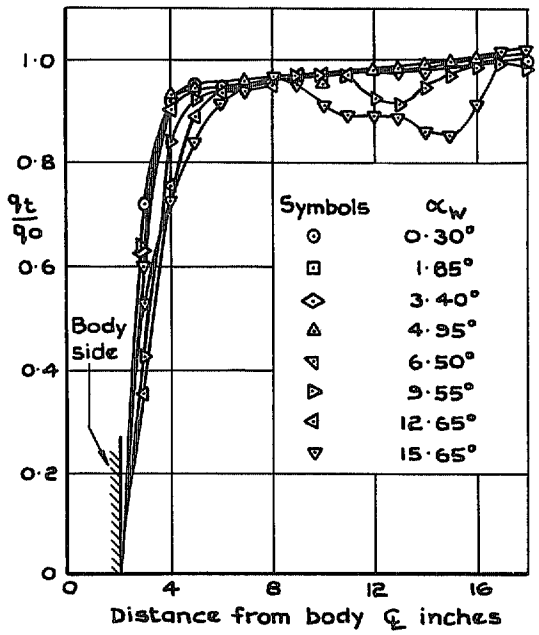

(a) Clean wing; low tailplane position

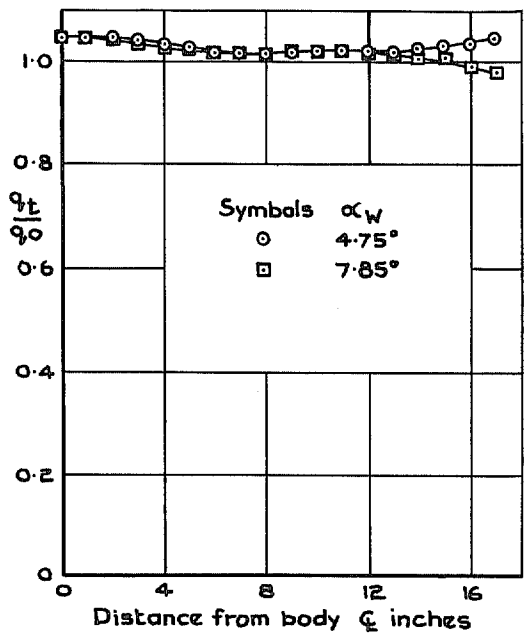

(b) Clean wing; flaps 35°, droop 25°, high tailplane position

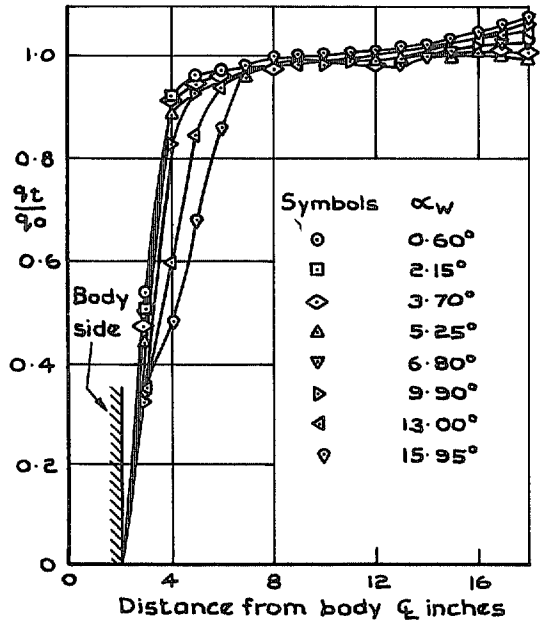

(c) Clean wing; flaps 35°, droop 25°, low tailplane position

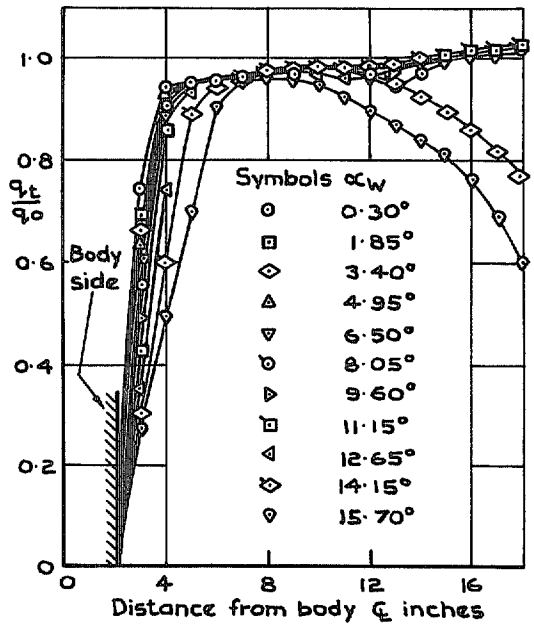

(d) Extended wing; low tailplane position

FIG. 23 a to d. Wake traverse on tailplane pivot line.

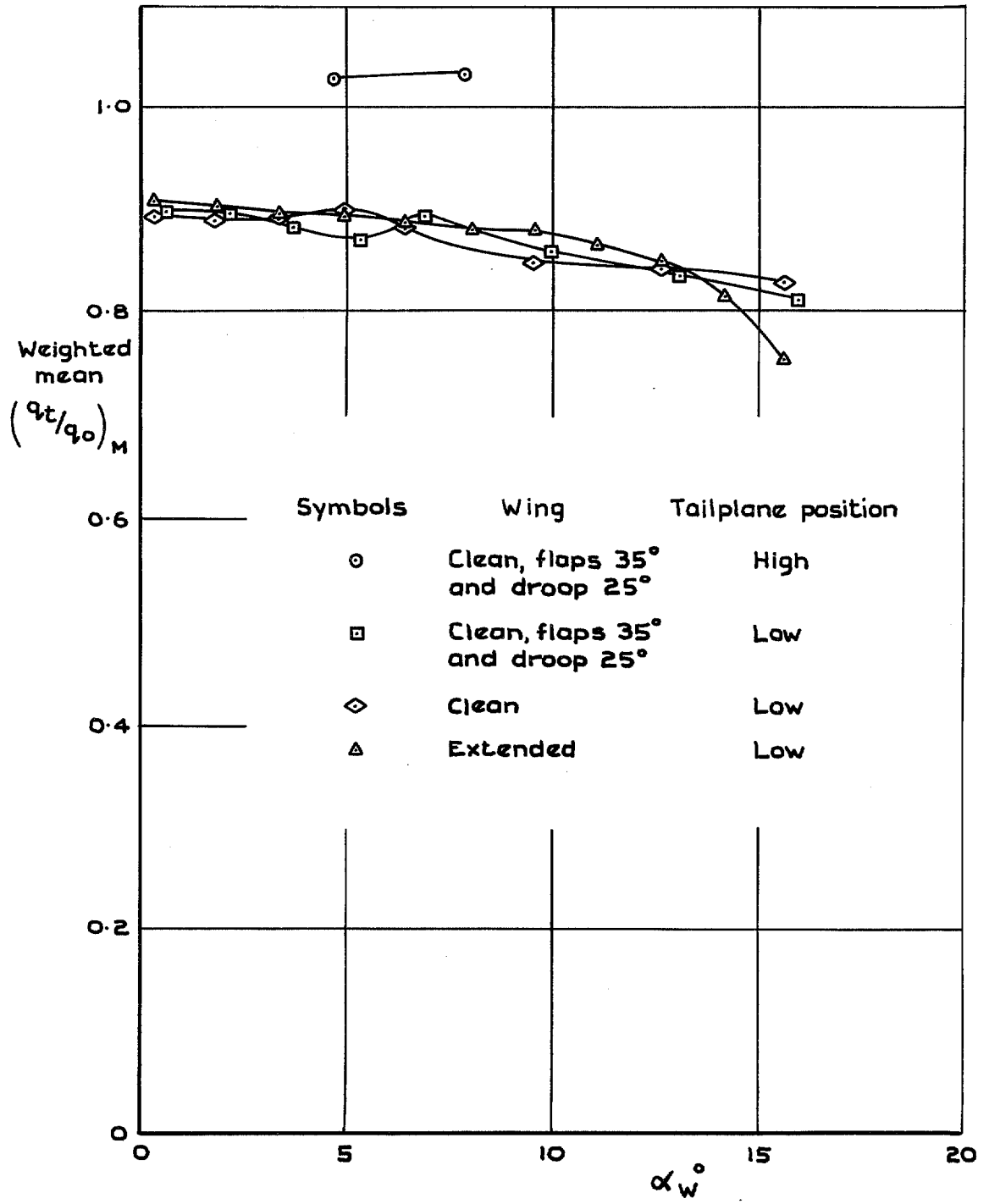

FIG. 24. Variation of weighted mean dynamic pressure at tailplane with incidence. Effect of wing condition and tailplane height.

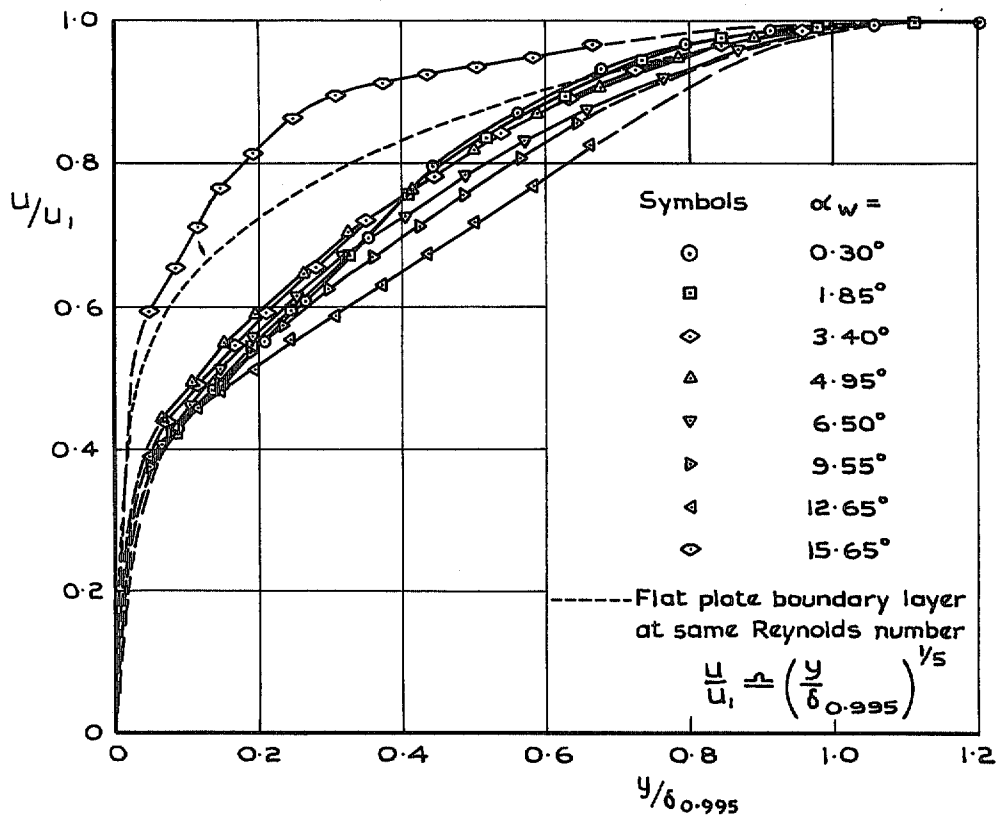

(a) Boundary-layer profiles

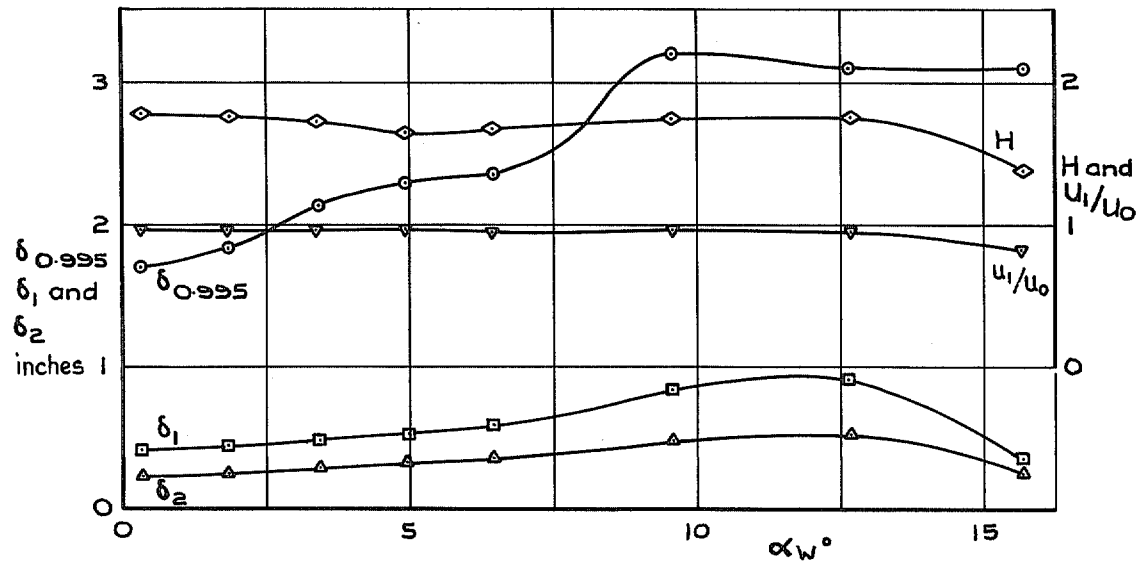

(b) Variation of boundary-layer thickness, shape parameter and u_1/u_0 with $\alpha_w°$

FIG. 25 a & b. Boundary-layer measurements on tailplane pivot line. Clean wing, low tailplane position.

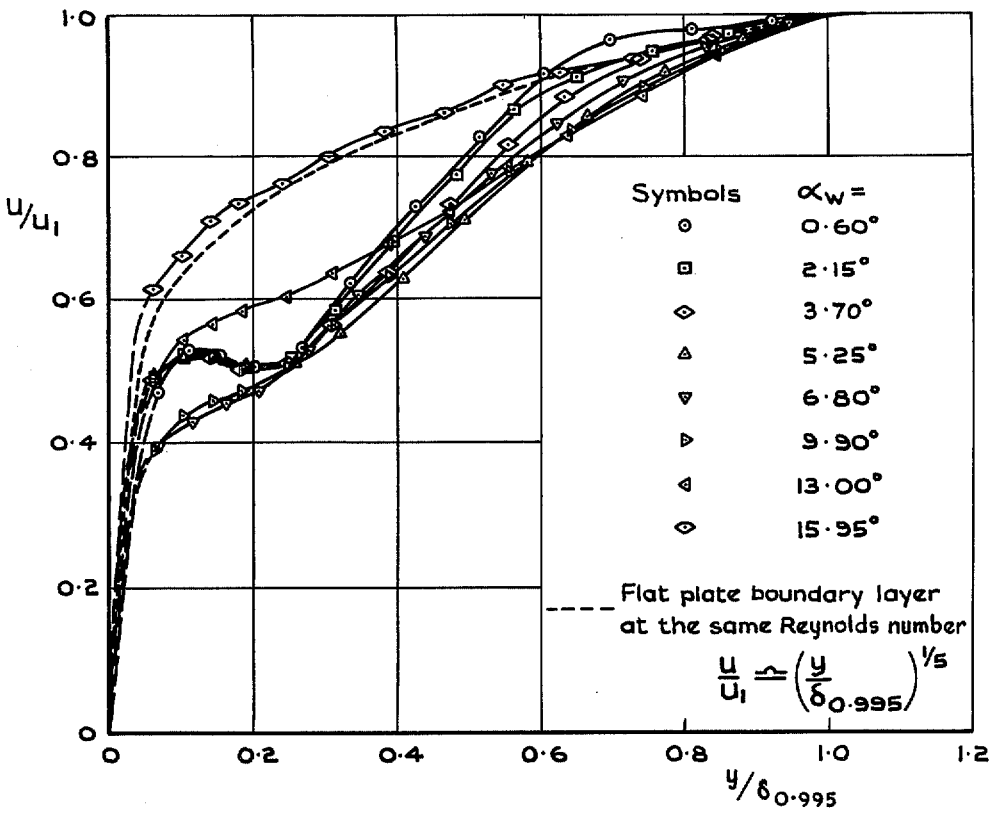

(a) Boundary-layer profiles

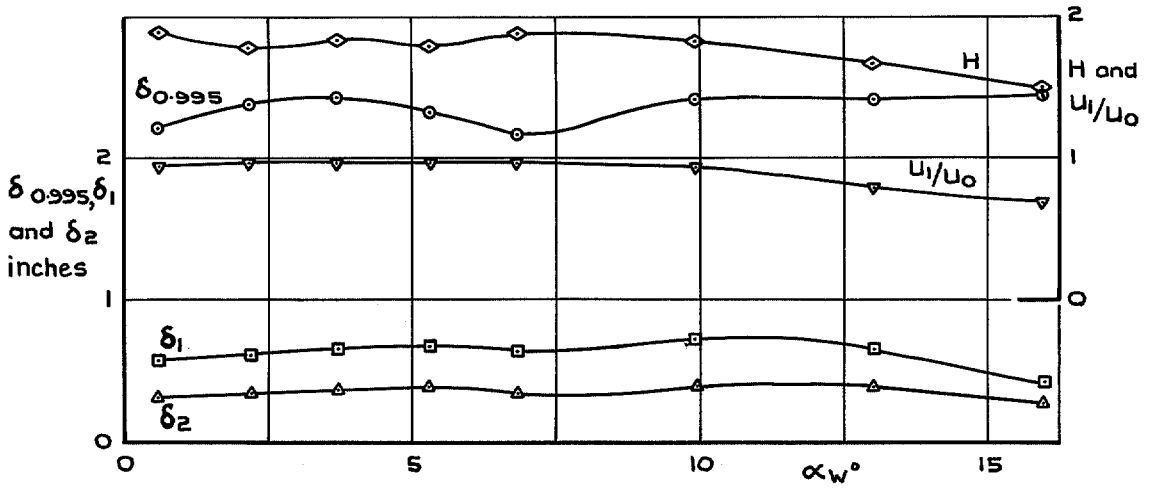

(b) Variation of boundary-layer thickness, shape parameter, and u_1/u_0 with $\alpha_w°$

FIG. 26 a & b. Boundary-layer measurements on tailplane pivot line. Clean wing, flaps 35° and LE droop 25°, low tailplane position.

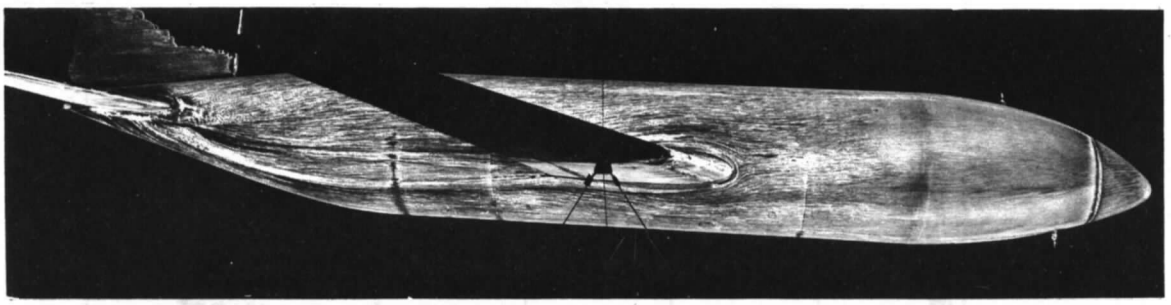

(a) $\alpha_w = -0.30°$

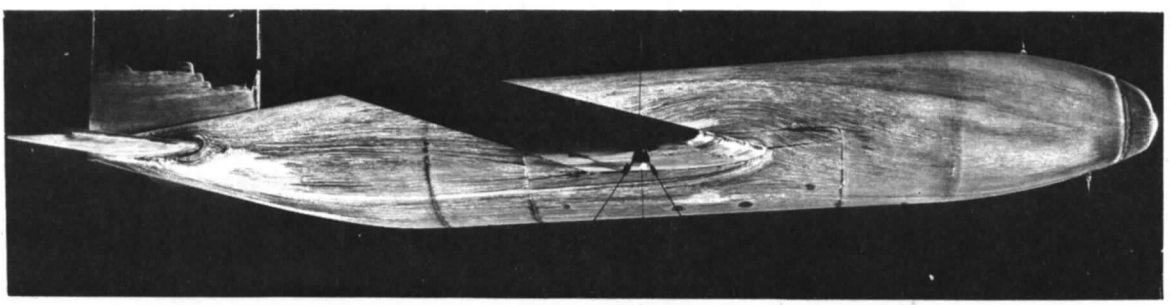

(b) $\alpha_w = 8.55°$

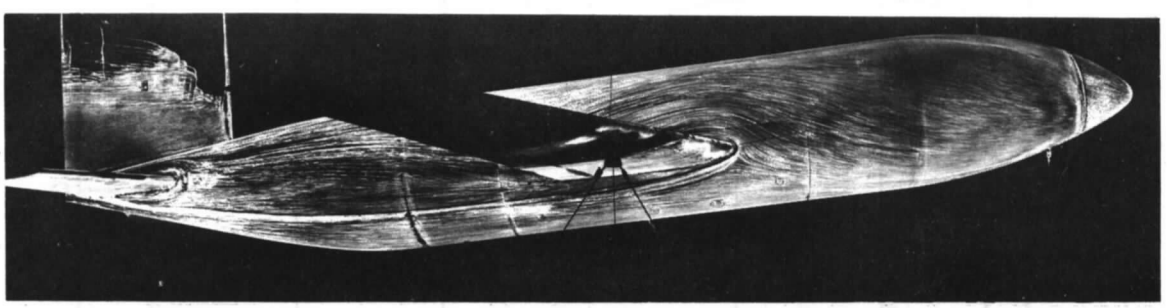

(c) $\alpha_w = 12.65°$

FIG. 27a to c. Flow visualisation on fuselage. Clean wing, low tailplane, $i_t = 0°$.

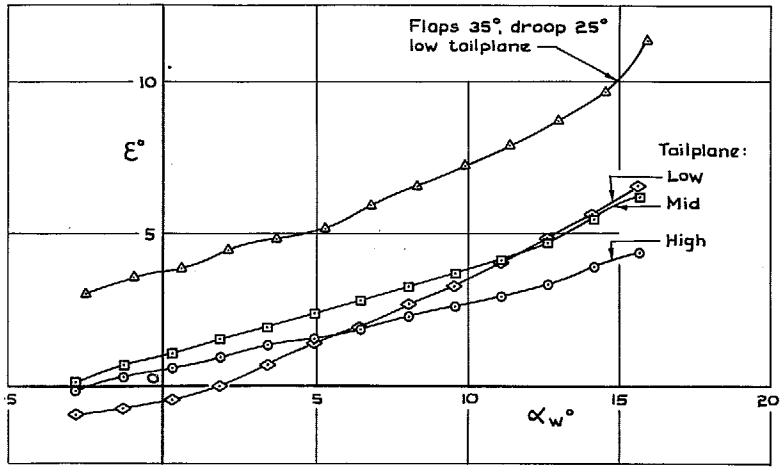

(a) Clean wing, with and without flaps

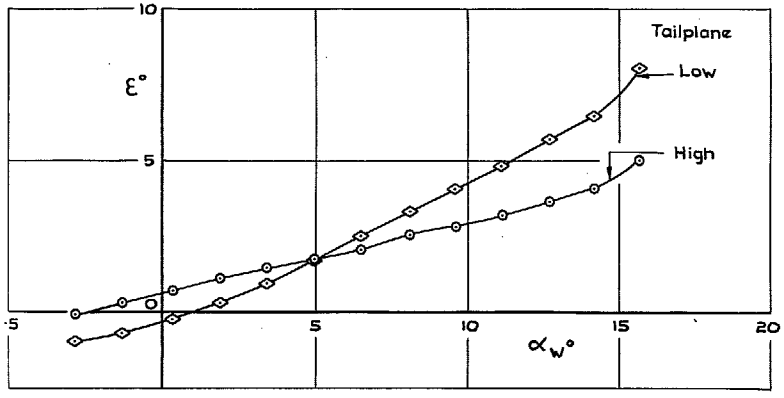

(b) Extended wing

FIG. 28 a & b. Derived downwash ε° *vs* α_w° for the clean and extended wing.

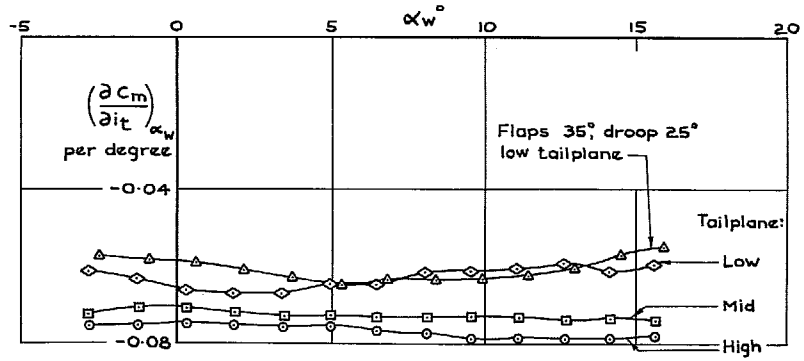

(a) Clean wing, with and without flaps

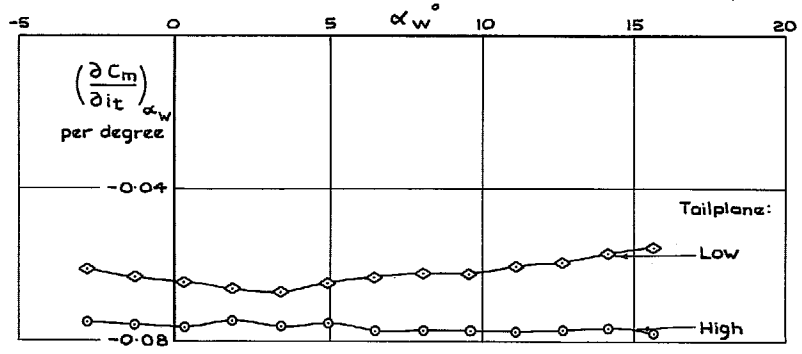

(b) Extended wing

FIG. 29 a & b. Measured $\left(\frac{\partial C_m}{\partial i_t}\right)_{\alpha_w}$ *vs* α_w° for the clean and extended wing.

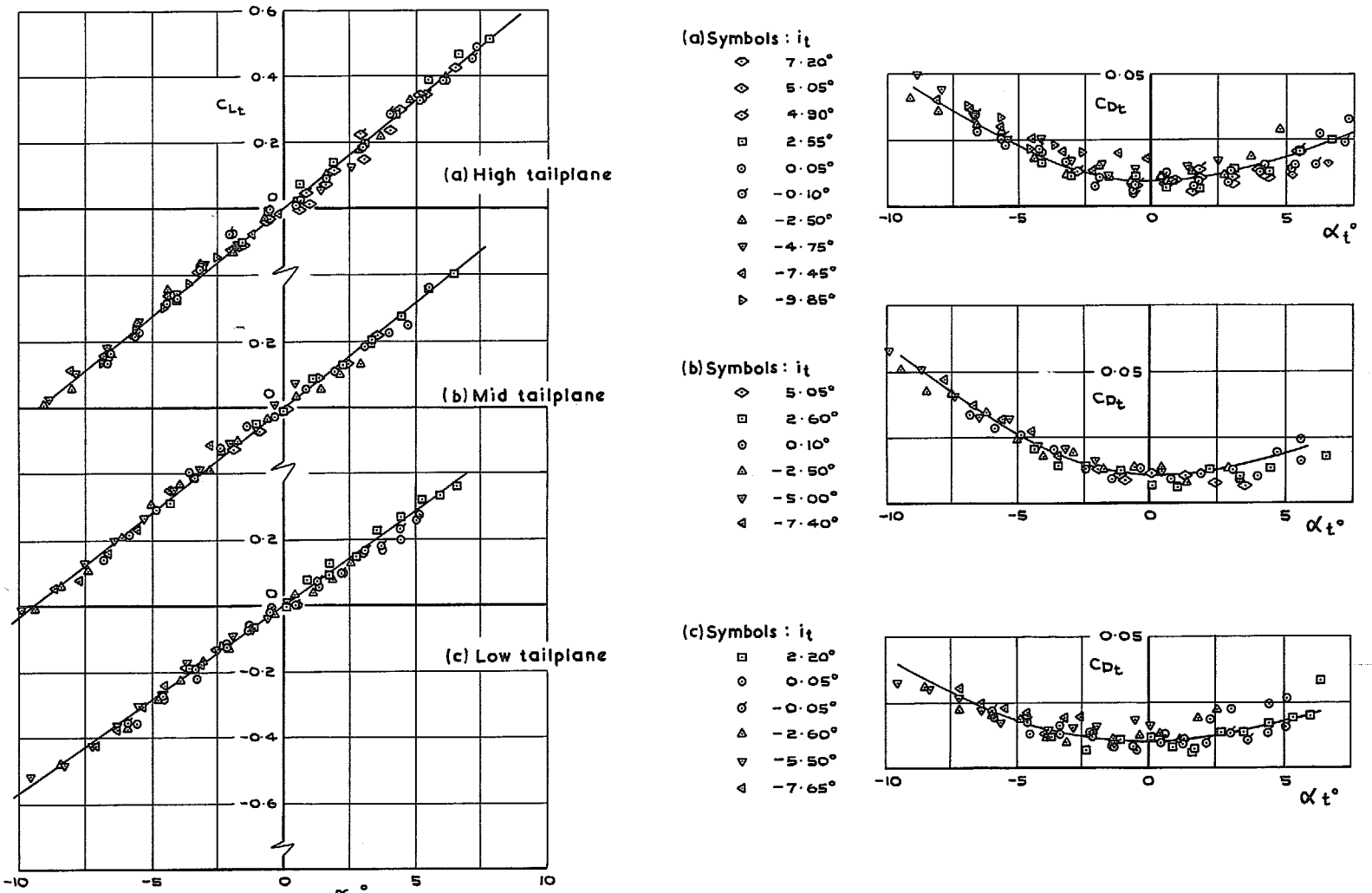

FIG. 30. Derived C_{L_t} and C_{D_t} *vs* $\alpha_t°$. Clean wing; three tailplane heights.

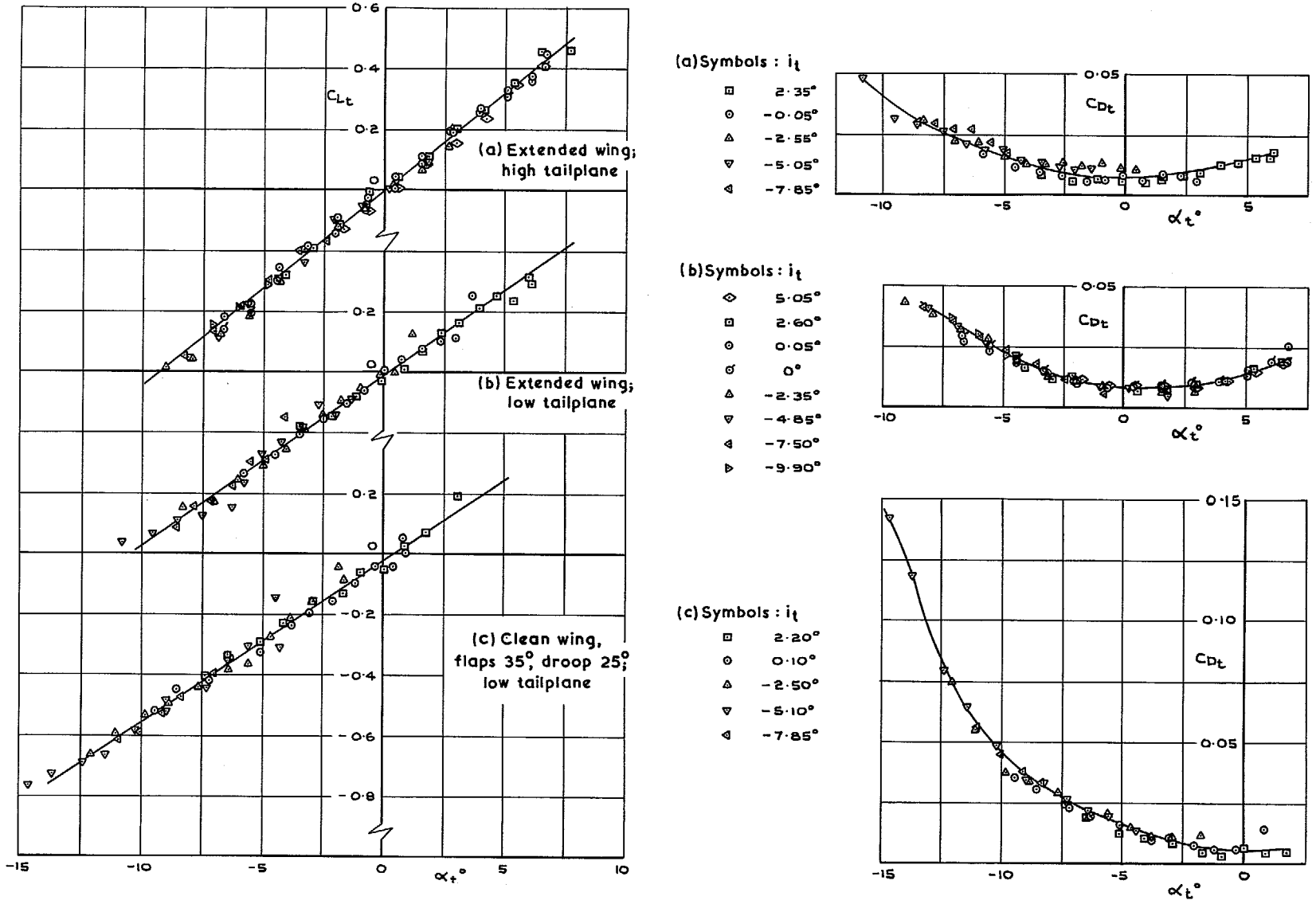

FIG. 31. Derived C_{L_t} and C_{D_t} *vs* $\alpha_t°$. Clean wing with flaps and extended wing.

Printed in Wales for Her Majesty's Stationery Office by Allens Printers (Wales) Ltd.
Dd.501372 K.5

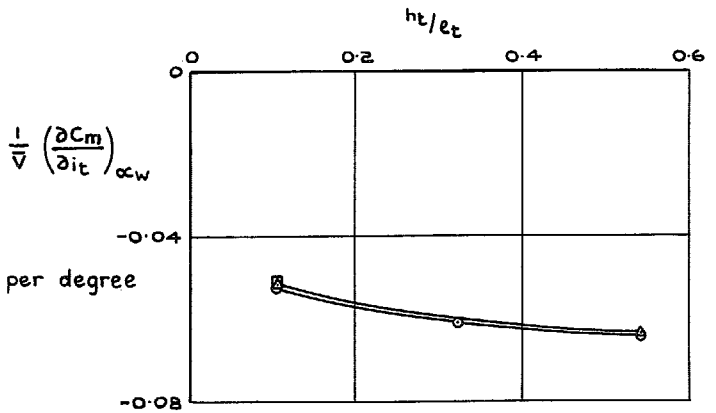

(a) As determined from the mean slope of the Cm vs it graph

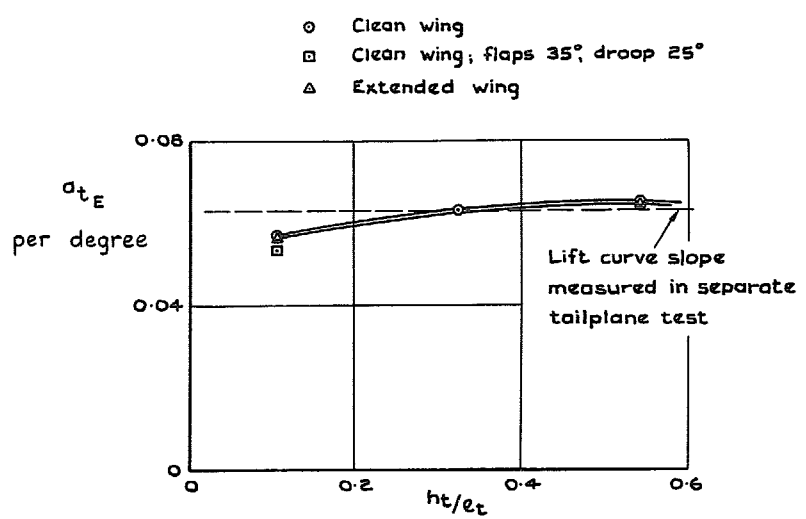

(b) As given by the effective tailplane lift curve slope

FIG. 32 a & b. Tailplane effectiveness for the clean and extended wings and three tailplane heights.

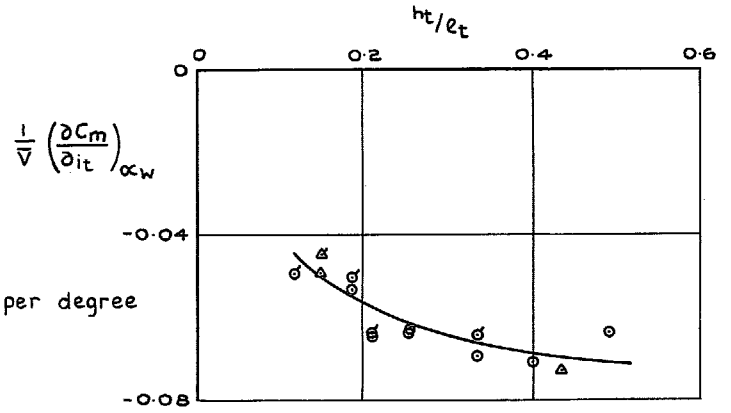

(a) As determined from the mean slope of the Cm vs it graph

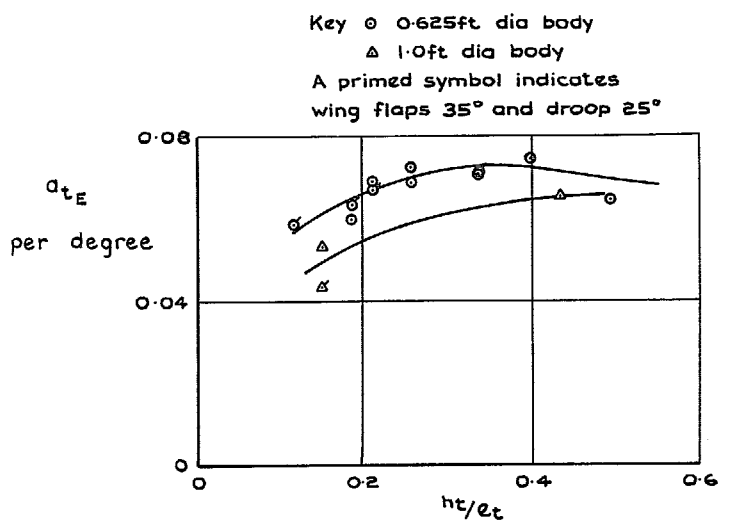

(b) As given by the effective tailplane lift curve slope

FIG. 33 a & b. Tailplane effectiveness for two body diameters and a range of the tailplane height to arm ratio (Model of Ref. 3).

Published by
HER MAJESTY'S STATIONERY OFFICE

To be purchased from
49 High Holborn, London WC1
13a Castle Street, Edinburgh EH2 3AR
109 St Mary Street, Cardiff CF1 1JW
Brazennose Street, Manchester M60 8AS
50 Fairfax Street, Bristol BS1 3DE
258 Broad Street, Birmingham 1
7 Linenhall Street, Belfast BT2 8AY
or through any bookseller

R. & M. No. 3642

SBN 11 470362 0